1 **Hippocampal Theta Phase Precession Supports Memory Formation**

2 **and Retrieval of Naturalistic Experience in Humans**

3

4 Jie Zheng[1], Mar Yebra[2], Andrea G. P. Schjetnan[3], Clayton Mosher[2], Suneil K. Kalia[3],

5 Jeffrey M. Chung[4], Chrystal M. Reed[4], Taufik A. Valiante[3], Adam N. Mamelak[2],

6 Gabriel Kreiman[1,5,*], Ueli Rutishauser[2,4,6,7,*]

7

8 [1] Department of Ophthalmology, Children's Hospital, Harvard Medical School, Boston,

9 MA, USA

10 [2] Department of Neurosurgery, Cedars-Sinai Medical Center, Los Angeles, CA, USA

11 [3] Krembil Research Institute and Division of Neurosurgery, University Health Network

12 (UHN), University of Toronto, Toronto, ON, Canada

13 [4] Department of Neurology, Cedars-Sinai Medical Center, Los Angeles, CA, USA

14 [5] Center for Brain Science, Harvard University, Cambridge, MA, USA

15 [6] Center for Neural Science and Medicine, Department of Biomedical Sciences, Cedars-

16 Sinai Medical Center, Los Angeles, CA, USA

17 [7] Division of Biology and Biological Engineering, California Institute of Technology,

18 Pasadena, CA, USA

19

20 *Correspondence to:

21 ueli.rutishauser@cshs.org and gabriel.kreiman@childrens.harvard.edu

22

23

Abstract

Linking different experiences together is a key aspect of episodic memory. A potential neural mechanism for linking sequential events over time is phase precession, which causes neurons to fire progressively earlier in time relative to theta-frequency local field potential oscillations. However, no direct link between phase precession and behaviorally assessed memory encoding or retrieval success has been established. We recorded the activity of single neurons and local field potentials in the human medial temporal lobe (MTL) while participants encoded and retrieved memories of movie clips. Transient brief theta bouts and theta phase precession were observed following cognitive boundaries during movie watching as well as following stimulus onset during memory retrieval. Phase precession was dynamic, with different neurons exhibiting phase precession in different task periods. The strength of phase precession provided information about memory encoding and retrieval success that was not available in firing rates, thereby linking the temporal code established by phase precession to behaviorally assessed memory strength. These data reveal phase precession during non-spatial memory in humans and provide direct neural evidence for a functional role of phase precession in episodic memory.

Introduction

From significant life events to mundane everyday moments, episodic memory plays a crucial role in shaping our perception of the world and our sense of self. Our brains not only store snapshots of individual events but also temporally weave together sequential contiguous moments into rich and coherent memories for future use. A fundamental open question in human memory is, how do we encode and retrieve memories of continuous experience?

Theoretical work suggests that the encoding, binding, and compressing of sequential events into a coherent memory might rely on a temporal neural code[1-4]. A key motivation for these theories is that the precise timing at which spikes of hippocampal neurons occur relative to ongoing field potential activity in the theta frequency range carries information about both the content of a given experience as well as the location of a given event within a sequence[5-9]. A key mechanism that gives rise to temporal coding is phase precession, whereby neurons spike in progressively

57   earlier phases of ongoing theta oscillations relative to the onset of either a significant

58   event[6,10] or the location of the animal in the case of place cells[11-13]. As a result of phase

59   precession, the phase of spiking relative to theta is indicative of the elapsed time since

60   the onset of the event. Phase precession was first discovered in rodents[11] and has since

61   been investigated extensively in the context of spatial coding of self[12] and others[14].

62   Phase precession has since also been reported in other species, including marmosets[15],

63   bats[16] and humans[17,18]. A key insight of the work in marmosets, bats, and humans is

64   that phase precession is robustly present even if the underlying theta activity is only

65   present intermittently in bouts[16]. Recent work further generalizes the presence of phase

66   precession towards non-spatial domains, demonstrating its relevance to auditory stimuli

67   identity encoding[6,19], odor identity encoding[6], time in an event sequence[20-22], and

68   sleep[20].

69

70   Despite its prevalence, the precise functional role that phase precession plays in

71   memory remains elusive. Phase precession coordinates hippocampal cell assemblies

72   such that different cells fire in order within a single theta cycle[13,23] in a manner that is

73   conductive to synaptic plasticity[2,24]. Recent rodent[6] and human studies[17,25] report that

74   phase precession occurs most strongly following event onsets or event transitions.

75   Based on these data, it has been hypothesized that a function of phase precession is to

76   organize neural activity such that a cohesive memory can be formed and later be

77   retrieved. However, so far no direct link between the extent of phase-precession and

78   episodic memory-related behavior has been established.

79

80   We examined whether phase precession strength is related to whether a non-

81   spatial episodic memory is encoded or retrieved in humans during continuous

82   semirealistic experience. Our results make three key contributions. First, we report non-

83   spatial phase precession in humans after event boundaries during naturalistic

84   experience. Second, phase precession also occurred during recognition memory and

85   order memory retrieval. Third, the strength of phase precession reflected participants'

86   memory encoding and retrieval success. Overall, our findings extend phase precession

87   to non-spatial episodic memory and demonstrate a direct link between phase precession

88   and memory behaviors in humans.

89

Results

Task and neural recording

22 subjects with drug-resistant epilepsy participated in the experiment (3 new participants in addition to the 19 for which we already published single-neuron but not field potential data[26]; Supplementary Table S1). The task consisted of three parts: encoding, scene recognition, and time discrimination (see *Methods*). During encoding, participants watched 90 movie clips of approximately 8s length each. Each clip was novel and consisted of either a single continuous shot (Fig. 1b, referred to as "no boundary clips") or several different shots separated by event boundaries (Fig. 1a, "boundary clips"). After watching all 90 clips once, participants performed two memory tests. During the scene recognition test (Fig. 1c), participants indicated whether the presented frame was "old" (from watched clips) or "new" (not watched) via button press. During the time discrimination test (Fig. 1d), order memory was evaluated by asking participants to indicate which one of two frames shown on the screen appeared earlier in time in the movie clips just watched. Patients performed well in both memory tests, with accuracy of 73% $\pm$ 10% and 70% $\pm$ 12% for scene recognition and time discrimination test, respectively (scene recognition: $p < 4\times10^{-4}$; time discrimination: $p < 3\times10^{-3}$; one sample *t*-test with respect to chance level). Participants were implanted with depth electrodes for clinical evaluation while performing the task (see participant demographics in Supplementary Table 1 and spike quality metrics in Supplementary Fig. 1).

We quantified phase precession using simultaneously recorded single-neuron activity and local field potentials (LFP) from microwire electrodes implanted in the hippocampus, amygdala, and parahippocampal gyrus (Fig. 1e and Supplementary Table 2), jointly referred to as the MTL. We also recorded data from three frontal areas, including orbitofrontal cortex (OFC), anterior cingulate (ACC), and pre-supplementary motor area (preSMA), which we analyzed to compare the prevalence of phase precession between the frontal lobe (in total 41 microwires, 433 neurons) and MTL (in total 50 microwires, 503 neurons).
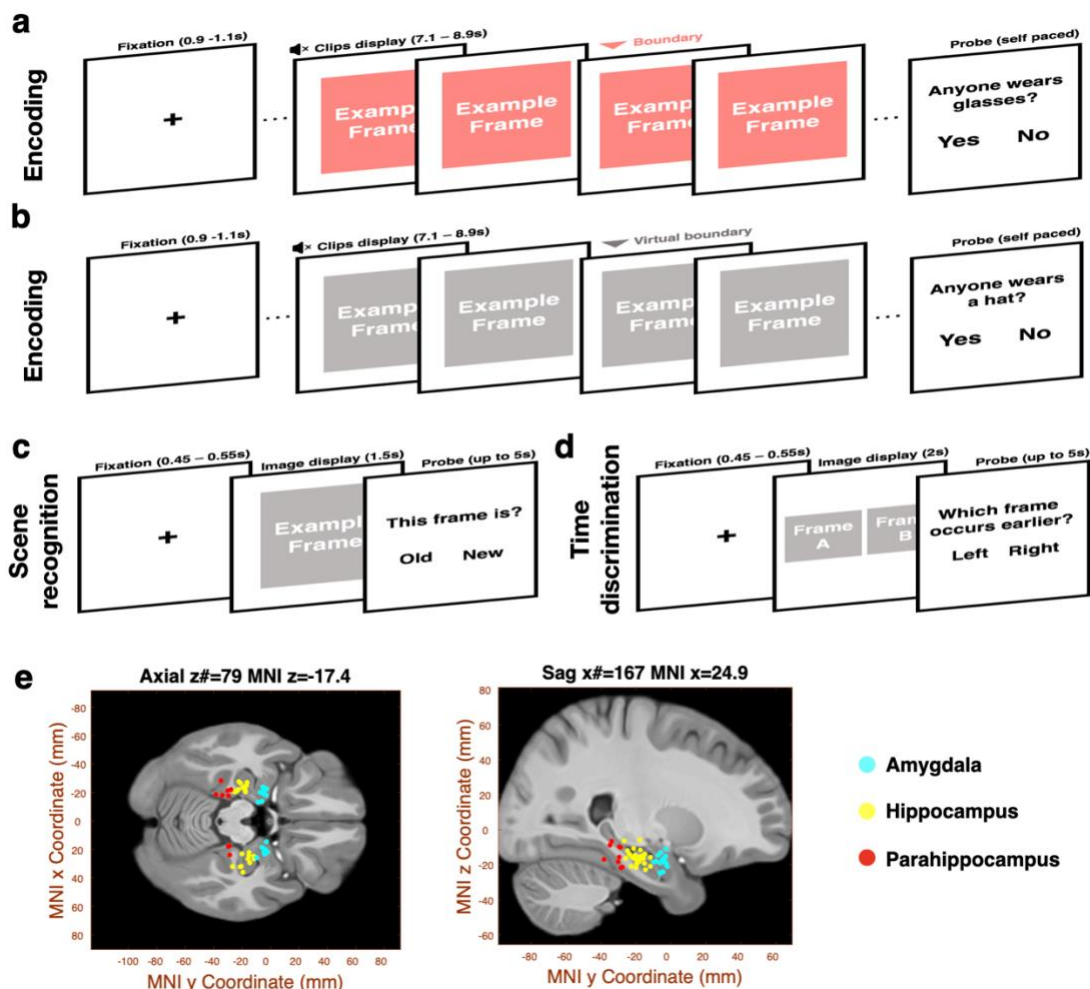
Fig. 1 | Experiment and electrode locations. (a-c) Schematics of the three task stages. **(a** and **b)** Encoding. Participants watched a series of silent clips and were instructed to answer yes/no questions that appeared randomly after every four to eight clips[26]. These clips either contained cuts to scenes from the same or different movie (a, boundary clips) or no cuts (b, no boundary clips). The red triangle in (a) marks the timepoint of the boundary in an example boundary clip. The gray triangle in (b) refers to the timepoint of 4 second in an example no boundary clip. **(c)** Scene recognition. Participants were presented with a static image and were asked to indicate whether the image was "old" (shown in the watched clips) or "new". **(d)** Time discrimination. Participants were presented with two images side by side and were asked to indicate whether the left or right frame appeared first in the watched clips. See[26] for more detailed information about the task. Due to copyright issues, all original images have been removed but are available upon reasonable request. **(e)** Illustration of the location of the 50 microelectrodes in the medial temporal lobe across 22 participants (see participants' demographics in Supplementary Table 1) that are included in this study. Shown is a slice from a template brain CIT168 (see *Methods*), with microelectrodes plotted as individual dots, and color-coded for different brain regions (Amygdala: cyan; Hippocampus: yellow; Parahippocampal gyrus: red). Montreal Neurological Institute (MNI) coordinates for all microelectrodes in the plot are listed in Supplementary Table 2.

Transient theta bouts in the MTL are prevalent following cognitive boundaries

140   As the internal reference "clock" for neuronal spiking[8], we first assessed the

141   properties of theta-band local field potentials (LFPs) recorded from the MTL (see

142   electrode locations in Fig. 1e and electrode Montreal Neurological Institute Coordinates

143   in Supplementary Table 2). Recordings from the amygdala, hippocampus, and

144   parahippocampal gyrus revealed large non-rhythmic fluctuations in the LFPs (Fig. 2a,

145   2c, 2e). Averaging power across the entire task, the LFPs recorded in these regions had

146   approximately $1/f$-shaped power spectra, with no apparent peaks in the conventional

147   theta range of 4-8Hz (Fig. 2a-f, Supplementary Fig. 2a-c and 2e-g).

148   We next searched for brief 'theta bouts' in the time domain on a cycle-by-cycle

149   basis[27] and quantified each oscillatory cycle by its amplitude, period and waveform

150   symmetry (see *Methods*). This analysis revealed transient "theta bouts" (see examples

151   highlighted in Fig. 2g and 2i; see *Methods*), consistent with previous findings in

152   humans[27-29] and other far-sensing species[15,16]. On average, 14% ± 4% of the entire

153   recording time was occupied by theta bouts. The likelihood of theta bout occurrence

154   varied across different task periods. During encoding, considering 1s long periods, theta

155   bouts were more likely to occur following cognitive boundaries in boundary clips (Fig.

156   2h; $F_{5,244}$ = 12.4, $p < 6\text{x}10^{-7}$; one-tailed ANOVA), with theta bouts occuping 36.4% ±

157   8.7% of post-boundary time windows. In contrast, theta bouts only occupied 16.2% ±

158   5.9%, 18.3% ± 4.7%, 16.8% ± 6.7%, 25.2% ± 8.8% and 15.6% ± 4.9% of the 1s long

159   time periods before cognitive boundaries in boundary clips, before and after no

160   boundaries in no boundary clips, after clip onsets and offsets in all clips, respectively.

161   The frequency of theta bouts was heterogeneous, spanning 2Hz to 10Hz. This was true

162   even when comparing different bouts detected on the same microelectrode (Fig. 2j and

163   2l shows two example microelectrodes). The variance of theta bout frequency changed

164   considerably across electrodes, with some electrodes having theta bouts with relatively

165   consistent frequencies (Fig. 2l, mostly from 6Hz to 8Hz). As a result, the

166   microelectrodes with relatively low variance in bout-by-bout frequency changes had

167   power spectra with prominent theta peaks when only considering the 1s period

168   following cognitive boundaries (Fig. 2k), whereas those with larger variance had at best

169   a modest peak (Fig. 2m). Across all electrodes, low variance was relatively rare, with

170   most electrodes exhibiting relatively large variance in the frequency of theta bouts (Fig.

171   2n; variance of theta bouts frequency for all the electrodes: 4.18 ± 1.14 Hz).
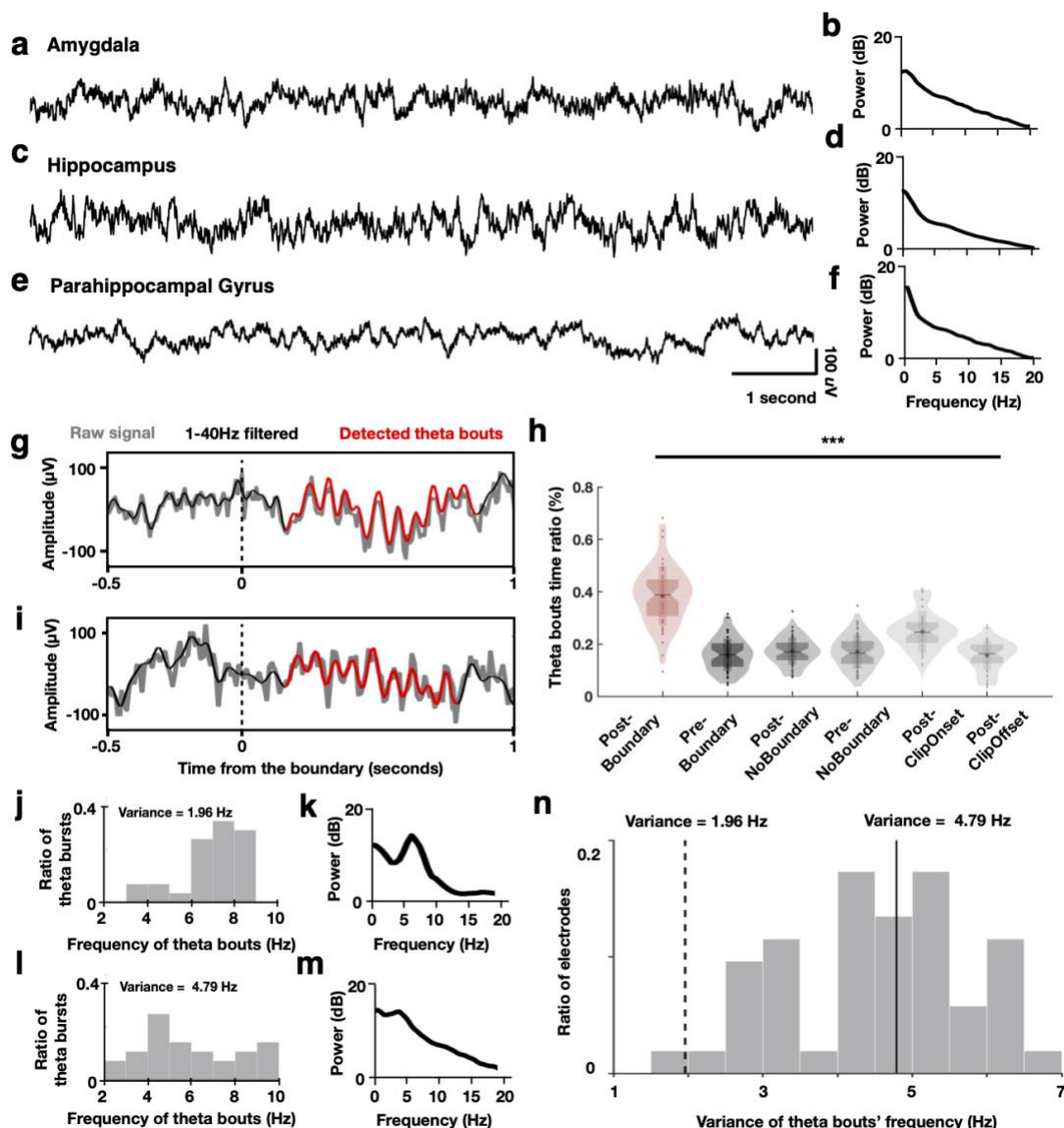
172

173

Fig. 2 | Characteristics of theta bouts during encoding. (a-f) Example local field potentials (LFPs) recorded from microelectrodes located in the amygdala (a), hippocampus (c), and parahippocampal gyrus (e). (b,d,f) LFP power spectra from the same example electrodes in a, c, e recorded throughout the entire task. **(g and i)** Examples of detected theta bouts. Shown is the raw LFP (gray), 1-40Hz bandpass filtered LFP (black), and detected theta bout (red). t=0 is the timepoint when a boundary occurs. **(h)** Proportion of time occupied by theta bouts within different 1-second time windows (analysis windows) before (Pre-Boundary) and after boundaries (Post-Boundary) in boundary clips, before (Pre-NoBoundary) and after (Post-NoBoundary) the midpoint in no boundary clips, after clip onsets (Post-ClipOnset) and clip offsets (Post-ClipOffset) of all the clips. Each dot represents one microelectrode. The shaded violin shape represents the data distribution with lower end of 1st percentile and top end of 99th percentile. The top edge and bottom edge of the shaded rectangle represents the mean + std. and mean – std., respectively. ***$p < 0.001$ (ANOVA test across all the analysis windows). **(j and l)** Frequency of all detected theta bouts within the Post-Boundary time windows for the two example microelectrodes shown in (g) and (i),

187 respectively. The inset shows the variance. **(k** and **m)** Power spectra of the LFPs across all the Post-

188 Boundary windows from the microelectrodes in (g) and (i), respectively. **(n)** Variance of the frequency

189 of theta bouts across all recorded microwires in the MTL. Solid and dashed lines mark the variance of

190 the two example microelectrodes shown in (g) and (i), respectively.

191

192   Consistent with the findings during encoding, theta oscillations during memory

193 retrieval were also relatively rare, resulting in approximately $1/f$-shaped power spectra

194 (Supplementary Fig. 2a-c and 3e-g). The incidence of theta bouts increased following

195 image onset in both retrieval tasks relative to baseline (Supplementary Fig. 2d and 2h; %

196 of time; scene recognition: $22.2\% \pm 6.3\%$ vs. $12.7\% \pm 3.8\%$; $F_{2,97} = 6.88$, $p < 2\text{x}10^{-3}$;

197 time discrimination: $21.6\% \pm 4.2\%$ vs. $14.2\% \pm 3.7\%$ $F_{2,97} = 7.11$, $p < 2\text{x}10^{-3}$; one-tailed

198 ANOVA). Theta bout prevalence was also relatively low during the later memory

199 retrieval periods (Supplementary Fig. 2d and h). Compared to encoding, the total time

200 occupied by theta bouts was substantially larger during encoding relative to that

201 following image onsets in both memory retrieval tasks (See Supplementary Fig. 2i;

202 encoding *vs* scene recognition: $36.4\% \pm 8.7\%$ *vs.* $21.3\% \pm 4.2\%$, $p < 1\text{x}10^{-5}$,

203 Kolmogorov-Smirnov test; encoding *vs* time discrimination: $36.4\% \pm 8.7\%$ *vs.* 22.4%

204 $\pm 6.2\%$, $p < 2\text{x}10^{-7}$, Kolmogorov-Smirnov test). Lastly, the frequency of detected theta

205 bouts following image onsets varied more compared to theta bouts following cognitive

206 boundaries during encoding (Supplementary Fig. 2j; scene recognition *vs* encoding:

207 5.25 ± 0.98 Hz *vs* 4.18 ± 1.14 Hz, $P < 2\text{x}10^{-3}$, Kolmogorov-Smirnov test; time

208 discrimination *vs* encoding: 5.47 ± 0.93 Hz *vs* 4.18 ± 1.14 Hz, $P < 1\text{x}10^{-4}$, Kolmogorov-

209 Smirnov test). In sum, these data show that LFPs in the human MTL contain prominent

210 but relatively rare and short transient bouts of activity in the theta range. Theta bouts

211 were most common following the occurrence of cognitive boundaries during encoding.

212

213 **Theta phase precession of individual neurons mostly occurs following boundaries**

214   Next, we examined whether the spiking of single neurons exhibited theta phase

215 precession during memory formation and retrieval of continuous experience. As theta

216 bouts occurred predominantly after boundaries during encoding (Fig. 2h), we started

217 by assessing phase precession within the post boundary windows in boundary clips.

218 Given the wide range of theta bout frequencies (Fig. 2n), we quantified phase

219 precession with respect to activity within a range of theta frequencies between 2 to

220 10Hz. Similar to the methods used in rodents[11,13,30], we quantified phase precession by

221   computing the circular correlation[31] between the theta phase of spikes and elapsed time

222   after boundaries within each microwire. We assessed the significance of phase

223   precession using a shuffle-based permutation procedure (see *Methods*). We quantified

224   elapsed time as the total accumulated theta phase rather than absolute time, a metric we

225   refer to as 'unwrapped phase' throughout. This is a common method to assess phase

226   precession first introduced by Mizuseki et al[32] and widely used in the context of

227   nonstationary LFPs[16,17]. For example, 0° in the x-axis in Fig. 3a marks the time of

228   boundary onset and 1080° marks the time after three cycles of theta have elapsed.

229

230

231   **Fig. 3 | Prevalence of theta phase precession across different task stages.** (**a**) Example hippocampal

232   phase precession neuron (detected from the microelectrode shown in Fig. 2g). The spiking of this neuron

233   exhibited phase precession after boundaries during encoding. The spiking phases relative to local theta

234   (y-axis) are plotted as a function of time in unwrapped theta phase (i.e., how many theta cycles have

235   passed, Methods). Each dot shows one spike within three theta cycles (1080 degrees on the x-axis)

236   relative to boundaries in boundary clips. The orange line indicates the fitted correlation between neuronal

237   spiking phase and time in unwrapped theta phase, with its correlation value (*r*) and significance level (*p*)

238   listed on top of the plot. (**b** - **d**) Distribution of correlation coefficients for all MTL neurons demonstrating

239   significant phase precession during encoding (b, orange), scene recognition (c, blue) or time

240   discrimination (d, green). Distribution of correlation coefficients for neurons without significant phase

241   precession is plotted in gray. Note that strong phase precession is indicated by negative correlation

242   coefficients. (**e**) Comparison of phase precession strength during encoding for phase precession neurons

243   in (b). Stronger phase precession is indicated by more negative correlations. Plotted are circular-linear

244   correlation coefficients computed using spikes fired within three theta cycles before (Pre-Boundary) and

245   after (Post-Boundary) boundaries in boundary clips, after clip onsets (Post-ClipOnset) and after clip

246   offsets (Post-ClipOffset) in boundary clips, also before (Pre-NoBoundary) and after (Post-NoBoundary)

247   the midpoint in no boundary clips. (**f** and **g**) Comparison of phase precession strength during scene

248   recognition (f) or time discrimination (g) for phase precession neurons in (c) and (d), respectively. Plotted

249   are circular-linear correlation coefficients computed using spikes fired within three theta cycles before

250   (Pre-ImageOnset) and after image onsets (Post-ImageOnset), after image offsets (Post-ImageOffset) and

251   after making a memory choice (Post-buttonPress). In (e-g), each dot represents one neuron. The shaded

252   violin shape represents the data distribution with lower end of 1st percentile and top end of 99th percentile.

253   The top edge and bottom edge of the shaded rectangle represent the mean ± std., respectively. ***$p<$

254   0.001 (one-sample t-test against zero), n.s. = not significant.

255

256   We found that 68/503 (13.5%; above chance, $p < 7x10^{-4}$, permutation test) of

257   neurons in the MTL demonstrated significant phase precession following cognitive

258   boundaries during encoding as assessed using this method ($p < 0.05$, permutation test;

259   see example in Fig. 3a and *Methods*). Fig. 3b shows the distribution of correlation

260   coefficients for the selected 68 neurons. As time elapsed following cognitive

261   boundaries, most phase precession neurons (66/68, 97%) spiked progressively earlier

262   relative to ongoing theta (from 360º to 0º), characterized by a negative spike-phase

263   correlation (Fig. 3b). Phase precession neurons exhibited an average correlation

264   coefficient of -0.38 ± 0.11 ($p < 3 \times 10^{-8}$, one-sample t-test), which is comparable to the

265   strength of phase precession reported previously (Feng et al, 2015; Terada et al, 2017;

266   Schmidt et al, 2009). By definition, phase precession neurons had more negative ($p <$

267   $3x10^{-4}$, Kolmogorov-Smirnov test) correlation coefficients compared to non-phase

268   precession neurons (-0.07 ± 0.13, mean ± std; $p = 0.26$, one-sample t-test). To evaluate

269   the robustness of phase precession, we also computed phase precession using two

270   alternative methods, which demonstrated consistent findings (Supplementary Fig. 3 and

271   Supplementary Table 3; see *Methods*).

272

273   Was phase precession specific to the 1s period of time following cognitive

274   boundaries? For the neurons showing phase precession after cognitive boundaries (n =

275   68, Fig 3b orange), phase precession strength was not significantly different from

276   chance for other periods of time during encoding (Fig. 3e). These findings suggest that

277   phase precession is present during memory formation of continuous experience

278   following cognitive boundaries.

279
280   **Phase precession is task dependent and anatomically specific**

281   We next turned to assessing phase precession during memory retrieval. We

282   found that 10.1% (51/503) and 17.7% (89/503) of MTL neurons showed phase

283   precession ($p < 0.05$, permutation test) when participants were presented with tested

284   images during scene recognition (Fig. 3c) and time discrimination (Fig. 3d),

285   respectively. These neurons exhibited an average correlation coefficient of -0.41 ± 0.09

286   ($p < 2 \times 10^{-8}$, one-sample t-test) during scene recognition and -0.40 ± 0.12 during time

287   discrimination. By definition, these correlation coefficients were more negative than

288   those of non-phase precession neurons (scene recognition: $p < 2 \times 10^{-4}$; time

289   discrimination: $p < 2 \times 10^{-4}$; Kolmogorov-Smirnov test). Similar to theta bouts, the

290   observed phase precession was prominent following the onsets of image display but not

291   during baseline, following image offset, and during the button press period (Fig. 3f and

292   3g).

293   We found that phase precession is a dynamic process. Among all the phase

294   precession neurons observed in the MTL across encoding, scene recognition, and time

295   discrimination (n = 117), half (61/117, 47.9%) demonstrated phase precession

296   exclusively for only one task stage (Fig. 4d; Fig. 4a-c shows an example). Of the

297   neurons that only showed phase precession in one task, the majority did so during time

298   discrimination (40/61, 65.6%) rather than encoding (18/61, 29.5%) or scene recognition

299   (3/61, 4.9%). We also observed neurons that showed phase precession during multiple

300   task stages (Fig. 4d; 56/117, 52.1%), with most of these neurons showing phase

301   precession for all three task stages (35/56, 62.5%). The strength of phase precession

302   varied across different task stages (see example in Fig. 4a-c), with more negative

303   correlations (indicating stronger phase precession) during the two memory retrieval

304   tasks compared to encoding (Fig. 4e and 4f, scene recognition – encoding: r_diff = -

305    $0.19 \pm 0.09, p < 3 \times 10^{-4}$; time discrimination – encoding: r_diff = $-0.24 \pm 0.11, p < 6 \times 10^{-7}$

306   ^{7}; one-sample t-test). Comparing the two retrieval tasks, phase precession was stronger

307   during time discrimination compared to scene recognition (time discrimination – scene

308   recognition: r_diff = $-0.11 \pm 0.04, p < 0.03$, one sample t-test). The observed differences

309   in phase precession strength could not be explained by differences in firing rates

310   because neurons had comparable firing rates across the three tasks (Supplementary Fig.

311   4a: scene recognition - encoding: Fr_diff = -0.18 ± 0.41 spikes/s, $p = 0.33$, one-sample

312   t-test; time discrimination - encoding: Fr_diff = -0.14 ± 0.38 spikes/s, $p = 0.24$, one-

313   sample t-test). Lastly, we asked whether phase precession strength varied as a function

314   of different types of trials within a given task. Phase precession during scene

315   recognition was significantly stronger following onset of images that were old

316   compared to images that were novel (-0.26 ± 0.14 vs. -0.11 ± 0.07, $p < 4$ x 10^{-3}, paired

317   *t*-test; see Supplementary Fig. 5), suggesting a role of precession in retrieval. Together,

318   these results indicate that the strength by which a given neuron exhibits phase

319   precession is a dynamic process that varies both as a function of the task and trial type

320   within the task.

321

322
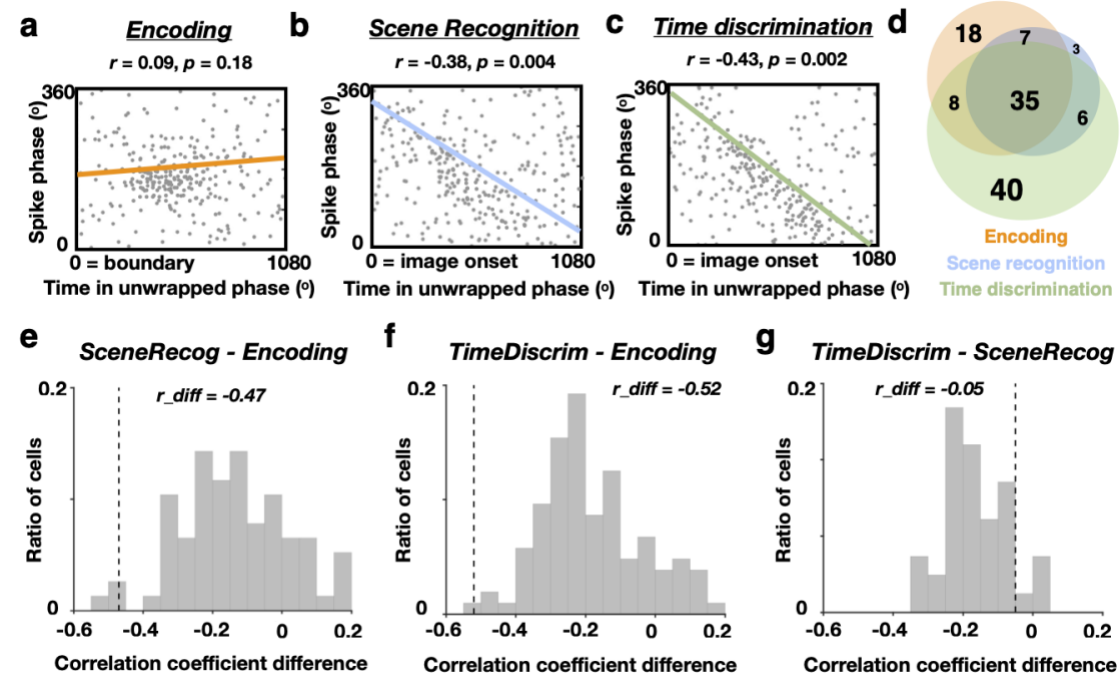
323   **Figure 4. Comparison of phase precession strength across different task stages.** (**a-c**) Example

324   hippocampal neuron whose spiking exhibited phase precession during recognition and time

325   discrimination, but not encoding. Shown are spike phases as a function of time in unwrapped theta phase,

326   displayed separately for encoding (a; t=0 is boundary in boundary clips), scene recognition (b; t=0 is

327   image onset) and time discrimination (c; t=0 is image onset). Colored lines indicate the fitted correlation

328   between spike phase and time in unwrapped theta phase. The correlation value (*r*) and its statistical

329   significance (*p*) are listed on top of each plot. (**d**) Number of MTL neurons showing significant phase

330   precession during encoding (orange), scene recognition (blue), time discrimination (green), and

331   combinations thereof. (**e**) Difference in phase precession strength between encoding and scene

332   recognition for neurons that show phase precession for encoding and/or scene recognition (i.e., orange

333   plus blue circles in panel d). (**f**) Difference in phase precession strength between encoding and time

334   discrimination for neurons that showed significant phase precession during encoding and/or time

335   discrimination (i.e., orange plus green circles in d). (**g**) Difference in phase precession strength between

336   scene recognition and time discrimination for neurons that showed significant phase precession during

337   recognition and/or time discrimination (i.e., blue plus green circles in d). Note that in (e-g), more negative

338   correlations indicate stronger phase precession. Dashed lines indicate the example hippocampal neuron

339   shown in (a-c).

340

341   We then asked how phase precession propensity varied across the brain. Only

342   the hippocampus and amygdala contained a significantly higher proportion of phase

343   precession neurons than expected by chance during all three task stages (Fig. 5a; $p <$

344   0.05, permutation test). While substantially rarer, the proportion of phase precession

345   neurons was also larger than expected by chance in the parahippocampal gyrus,

346   orbitofrontal cortex, and anterior cingulate cortex, but only during encoding and not

347   during either of the memory retrieval tests (Fig. 5a; $p < 0.05$, permutation test).

348

349
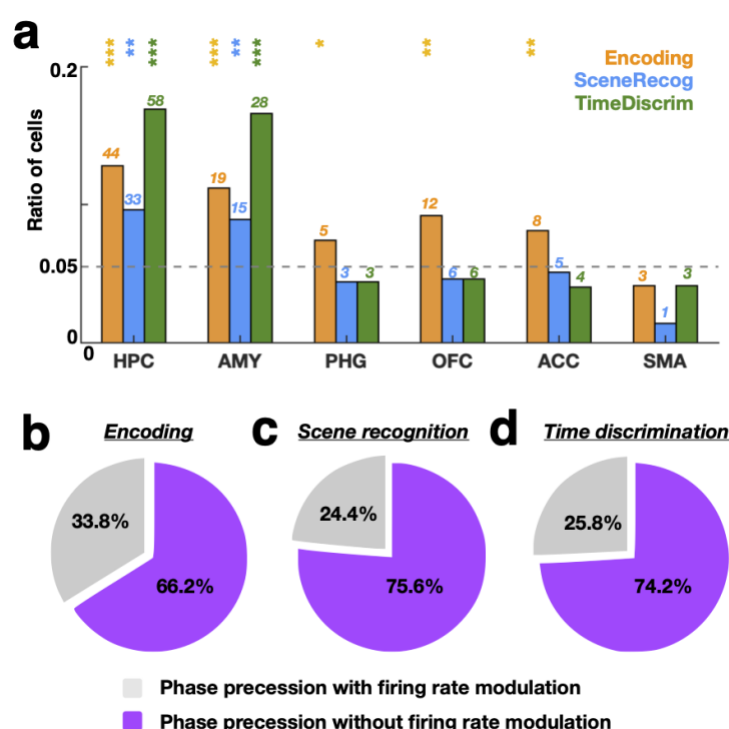
350   **Figure 5. Anatomical distribution of phase precession neurons and their co-occurrence with firing**

351   **rate changes. (a)** Phase precession was most prominent in MTL. Bars demonstrate the proportion of

352   neurons that exhibited phase precession in each anatomical area during different task stages (orange:

353   encoding; blue: scene recognition; green: time discrimination). The number of phase precession neurons

354   in each anatomical area is listed on the top of each bar. Dashed horizontal line indicates the chance level.

355   Asterisks mark brain areas under specific task stage with proportions of phase precession neurons larger

356   than expected by chance ($p < 0.05$, binomial test). HPC = hippocampus, AMY = amygdala, PHG =

357   parahippocampal gyrus, OFC = orbitofrontal cortex, ACC = anterior cingulate, SMA = supplementary

358   motor area. (**b**) Most phase precession neurons did not exhibit modulation by firing rate. Shown is the

359   proportion of phase precession neurons in MTL with/without firing rate modulation (defined as firing

360   rate differences between before vs. after boundaries during encoding). (**c** and **d**) Same as (b) but assessing

whether neurons changed their firing rate when comparing before and after image onset during scene recognition (c) or time discrimination (d). ***$p < 0.001$, **$p < 0.01$, *$p < 0.05$, n.s. = not significant.

Distinct phase and rate coding

We previously showed that a subset of MTL neurons selectively increased their firing rates after cognitive boundaries during encoding (we labeled these cells 'cognitive boundary cells', Zheng et al 2022). Were the phase-precessing neurons we describe here also cognitive boundary cells? On average, phase precession neurons had higher firing rates compared to non-phase precession neurons following onset of cognitive boundaries, indicating that the two groups of neurons might overlap (Supplementary Fig. 4b-4d). However, most of the phase precession neurons (encoding: 45/68, 66.2%) were not cognitive boundary cells (Fig. 5b). Similarly, during scene recognition and time discrimination, most phase precession cells did not change their firing rate following stimulus onset relative to baseline (Fig. 5c, scene recognition: 39/51, 76.5%; Fig. 5d, time discrimination: 66/89, 74.2%).

Phase precession strength predicts participants' memory performance

Given the largely separate groups of cells exhibitng phase precession and firing rate changes, we asked whether phase precession and firing rate provided complimentary information about memory encoding and/or retrieval success as assessed behaviorally. We tested this idea by computing phase precession strength (correlation coefficient) and average firing rates (normalized to baseline) separately for trials with correct and incorrect memory (see *Methods*). We then quantified how well phase precession strength and/or firing rates explained participants' memory performance (correct vs incorrect) using a generalized linear model. Based on comparisons between models with different combinations of features, we found that the winning model for explaining recognition memory performance is the model that has access to the three variables, phase precession strength during encoding, phase precession strength during retrieval, and firing rate during encoding (Fig. 6a, winning model marked in red). This model performed better than one with only access to firing rate. Similarly, for explaining time order retrieval performance, the winning model was also the one with access to all four variables (Fig. 6b; winning model marked in red). Further examining the winning models (marked in red in Fig. 6a and 6b) revealed that

394   in both instances, phase precession strength explained most variance compared to the

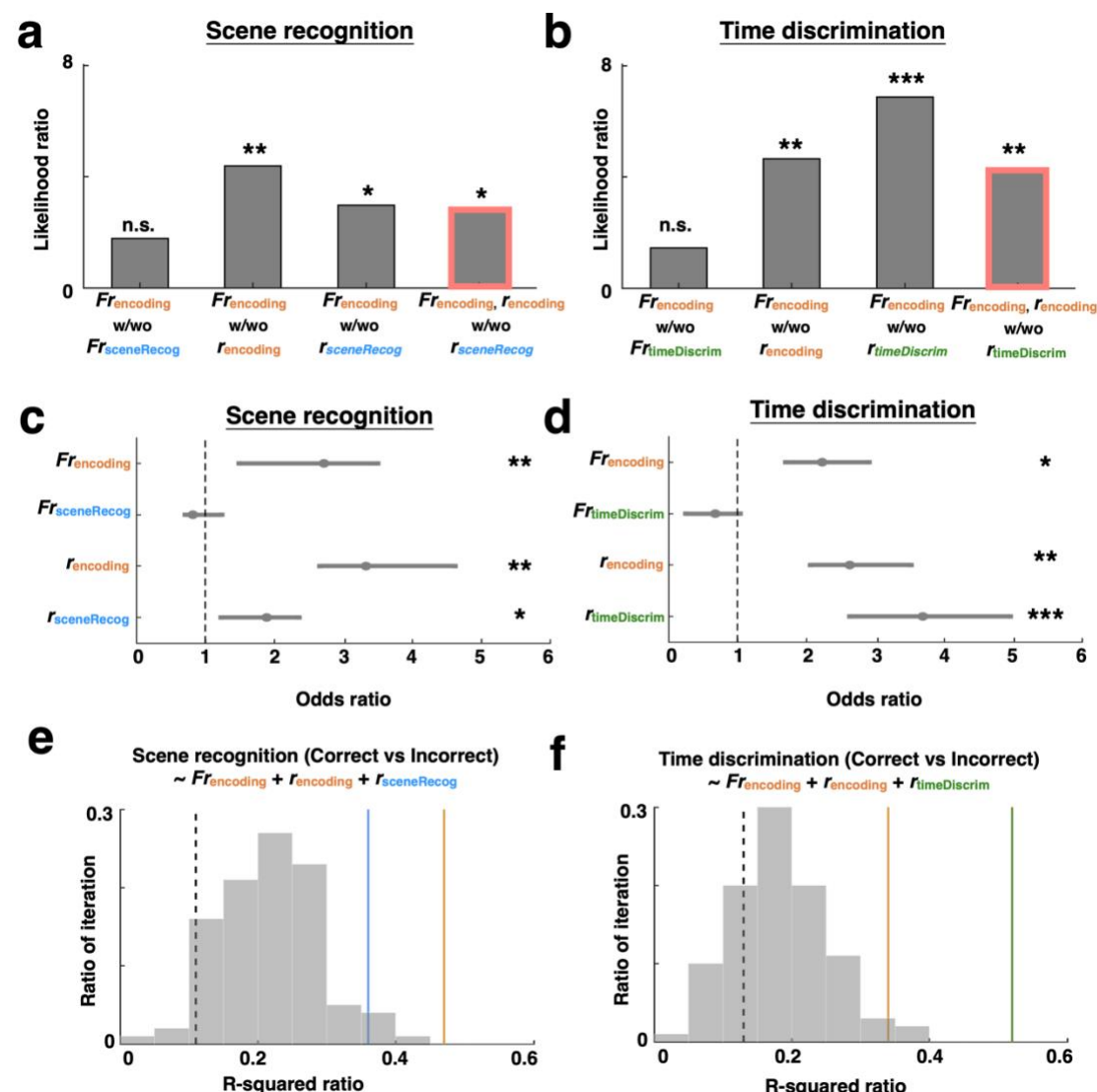395   firing rates (Fig. 6c-d).

396

397

398   **Figure 6. Strength of phase precession is predictive of memory encoding and retrieval success. (a)**
399   Model comparisons for neural activity during scene recognition task. Each bar shows a comparison
400   between the full GLM model and reduced GLM models with/without a given predictor. Likelihood ratio
401   bigger than 1 with significant p-value indicates a better model performance in explaining participants'
402   behavior outcomes with the added predictor. Predictors considered are firing rate during encoding
403   ($Fr_{encoding}$) and scene recognition ($Fr_{sceneRecog}$), and phase-precession strength during encoding ($r_{encoding}$)
404   and scene recognition ($r_{sceneRecog}$). (**b**) Same as (a), but for the time discrimination task. Predictors
405   considered are firing rate during encoding ($Fr_{encoding}$) and time discrimination ($Fr_{timeDiscrim}$), and phase
406   precession strength during encoding ($r_{encoding}$) and time discrimination ($r_{timeDiscrim}$). All the models in (a
407   and b) consider all the recorded neurons in the medial temporal lobe. (**c and d**) Odds ratios for different
408   predictors when predicting participants' memory performance during scene recognition (c) and time
409   discrimination (d). The ends of the horizontal lines indicate the confidence level and asterisk denote

significance (Waldon test). (**e**) For the winning model for scene recognition (indicated by red box in panel a), the proportion of variance in the response variable (correct vs incorrect) explained by different groups of neurons. Shown are R-squared ratios of models built using all phase precession neurons during encoding (orange line), all phase precession neurons during scene recognition (blue line), and all non-phase precession neurons. The total number of neurons used for the GLM model for each group are balanced by random subsampling. To do so, the non-phase precession neuron group is subsampled 100 times, each time selecting the same number of neurons as the number of phase precession neurons present during scene recognition. Dashed line indicates the chance level. (**f**) Same as €, but for time discrimination. Shown is the proportion of variance in the behaviour explained by the winning model (indicated by red box in panel b). Shown are model fit for all phase precession neurons selected during encoding (orange), all phase precession neurons selected during time discrimination (green), and all other neurons (grey, subsampled 100 times and each time with the same number of neurons as those selected during encoding). Dashed line indicates the chance level. * $p < 0.05$, ** $p < 0.01$, *** $p < 0.001$, n.s. = not significant.

Next, we assessed how much variance in the winning models was explained by subsets of the neurons (the results in above paragraph are for all recorded neurons). Compared to the rest of the MTL neurons, phase precession neurons explained significantly more variance in the behavioral accuracy during scene recognition (correct vs incorrect), with phase precession neurons during encoding and scene recognition exceeding 100% and 96% of the R-squared values achieved for random subsets of the same number of non-phase precession neurons (Fig. 6e), respectively. Similarly, phase precession neurons also explained the most variance in time discrimination accuracy, with phase precession neurons during encoding and time discrimination exceeding 97% and 100% of the R-squared values achieved for random subsets of the same number of non-phase precession neurons (Fig. 6f), respectively. In sum, the strength of phase precession provided information about memory encoding and retrieval success that was complementary to the information provided by firing rates, thereby revealing a temporal code.

Discussion

Theta phase precession is widely observed across species and is thought to be a neural mechanism to temporally link continuous experience and encode and retrieve these experiences into and from memory[11]. However, how phase precession facilitates memory formation and retrieval remains an open question that requires more direct neural evidence. Here we test the hypothesis that phase precession supports memory

formation and retrieval of naturalistic experience in humans. We found that phase precession was prominent following cognitive boundaries during movie clip watching and when participants retrieved memories of the content and temporal structure of the previously watched movie clips. The strength of phase precession was predictive of participants' ability to encode and retrieve the memories.

Theta phase precession was prominent despite the absence of long and continuous stretches of theta activity like that observed in rodents. This observation is consistent with work in bats, where phase precession is also prominent despite theta only being present in short bouts[16] similar to those in humans. Consistent with previous work[27,28], theta-frequency band LFP fluctuations in humans tend to be non-rhythmic, except for short transient theta "bouts" (Fig. 2). The frequencies of theta bouts detected on the same recording electrode can vary across a broad range (2-10Hz; Fig. 2i), which is in line with previous observations in humans[17] and bats[16]. Theta bouts and theta phase precession are both prevalent after cognitive boundaries during encoding (Fig. 2h and Fig. 3e) and image onset during retrieval (Supplementary Fig. 2d and 2h, Fig. 3f and 3g). However, the strength of phase precession does not solely depend on theta periodicity. Illustrating this, phase precession is stronger during memory retrieval compared to encoding despite theta bouts being rarer and variable during retrieval compared to encoding (see Supplementary Fig. 2i and 2j). Previous studies have also reported phase precession when theta frequency is altered[33], theta-modulated spiking is reduced[34-36], or even with little periodicity of low-frequency field potentials[15,16]. Moreover, theoretical work shows that periodicity is not necessary for phase precession[37]. Indeed, recent work suggests unique advantages of phase coding in the absence of rhythmicity, which enables multiplexing of rich information through a broad range of oscillatory frequency[38]. Our results, together with previous literature, support the idea that phase precession can serve as a flexible neural coding principle that is effective for both narrow- and broadband theta.

What triggers phase precession? We observed the strongest phase precession following cognitive boundaries during encoding and following image onset during scene recognition and time discrimination (Fig. 3c, 3f and 3g). Both cases contain sharp visual transitions, either across two different movie scenes or from a blank screen (baseline) to a movie scene. However, not all sharp visual transitions trigger phase

precession, as phase precession following movie clip onsets, movie clip offsets, image offsets, and button presses was not different from that expected by chance (Fig. 3c, 3f and 3g). We therefore posit that phase precession occurs when encoding or retrieving memories across events within a continuous experience. This hypothesis is consistent with previous findings[6,25] that show phase precession at event transitions in discrete event sequences.

The strength of phase precession varied across the different task stages. As stated above, stronger phase precession was observed during scene recognition and time discrimination compared to encoding (Fig. 4e and 4f). Also, during recognition memory, phase precession was stronger in old compared to new trials. We posit that these differences in phase precession strength might be the result of memory-based decision making, during which the precise temporal structure of previous experiences is relevant. Supporting this hypothesis, more phase precession neurons (Fig. 4d) were found during time discrimination compared to scene recognition. Also, stronger phase precession (Fig. 4g) was more predictive of participants' order memory accuracy compared to recognition memory accuracy (Fig. 6c and Fig. 6d). A previous study[39] has also reported stronger phase coding (but not phase precession) when animals were instructed to make a memory-based decision compared to passively trespassing the same environment.

A potential explanation of changes in phase precession strength between tasks could be the different strategies participants used when solving the two memory tests. During time discrimination, participants needed to determine the order of the two frames shown on the screen, which requires recollection of the entire event sequence. In contrast, during scene recognition, participants only needed to retrieve the memory associated with a single image. Notably, during scene recognition, phase precession is mostly observed during trials in which an old (familiar) image was shown (Supplementary Fig. 5). Identification of novel (foil) images might not require phase precession because it could rely on novelty signals[40,41]. An important future question is what the relationship is between phase precession and other forms of neural coding, such as novelty [40]. The dynamic task-dependent phase precession strength observed in our study suggests that phase precession can serve different functional roles as needed.

514   Models with access to both phase precession strength and firing rate were able

515   to explain variance in behaviorally assessed memory accuracy of the participants

516   significantly better than models with access to firing rate alone (Fig. 6). This finding

517   supports the idea that phase information provides information that trial-averaged firing

518   rate does not provide, making the two codes complementary[42,43]. Combining both rate

519   and phase coding, hippocampal cell assemblies may generate sequential structures

520   across single theta cycles that represent sequences of past, current, and future states in

521   both the spatial and episodic domain in a compressed manner[12,13,44]. While phase

522   precession has largely been reported for neurons with known tuning curves (i.e., rate

523   coding, such as place cells and grid cells), most phase precession neurons in our study

524   did not show modulation of firing rate with the variables examined in this study (Fig.

525   5b-d). This independence of phase precession strength and firing rate modulation is

526   consistent with theoretical models[43,45], and previous observations in rodents[46] and

527   humans[17] that show that phase precession can appear in the absence of concurrent firing

528   rate changes. An alternative interpretation is that we did not test for the variables that

529   would modulate firing rate in these neurons. Even for the subgroup of neurons which

530   showed both significant firing rate changes and phase precession, our findings differed

531   from those of place cells (which exhibit both rate and phase coding). This is because in

532   our study, all movie clips are shown only once (they are novel). Contrary to place

533   cells[11], the rate tuning of phase precession neurons in our study is thus not tied to a

534   specific stimulus. These findings suggest that phase precession in a given neuron can

535   occur during exposure to many different novel stimuli that have the occurrence of

536   cognitive boundaries in common, thereby flexibly capturing the temporal structure of

537   diverse event sequences using a shared neural coding mechanism.

538

539   In sum, we demonstrate non-spatial phase precession during memory formation

540   and retrieval of naturalistic experience in humans. The strength of phase precession and

541   the groups of neurons showing phase precession are task specific and the strength of

542   phase precession was predictive of the success of memory encoding and retrieval above

543   and beyond firing rates alone. Our findings suggest that phase precession in humans is

544   a general neural coding mechanism that can flexibly support different aspects of

545   episodic memory.

546

547

Methods

Task

The task (Fig. 1a-d) consisted of three parts: encoding, scene recognition, and time discrimination. During encoding, participants watched 90 novel and silent clips embedded with or without boundaries, defined as movie cuts transitioning to scenes from the same or different movie. To assess attention, a yes/no question related to the content of the clip appeared randomly after every 4-8 clips. After watching all 90 clips, participants were instructed to take a short break, roughly 5 minutes, before proceeding to the memory tests. Participants first performed the scene recognition test and were instructed to identify extracted frame from watched clips as "old" and novel frames as "new". Participants then performed the time discrimination test to identify whether the "Left" or "Right" frame was shown first (earlier in time) during encoding. More detailed information about the task design can be found in our previous publication [26].

Participants:

Twenty-two patients (13 females, mean age = 39 ± 16 years, mean ± s.t.d, see participants' demographics in Supplementary Table 1) with refractory epilepsy volunteered for this study and provided their informed consents. Nineteen of these participants come from our previous work [26] and there are three new participants. Participants performed the task while they stayed at the hospital and were implanted with electrodes for seizure monitoring. The study protocol was approved by the Institutional Review Boards at Toronto Western Hospital and Cedars-Sinai Medical Center. The location of the implanted electrodes was solely determined by clinical needs.

Electrophysiological recordings

Broadband neural signals (0.1 – 8000Hz filtered) were recorded using Behnke-Fried electrodes (Fried et al., 1999) (Ad-Tech Medical, Wisconsin, USA) at 32KHz using the ATLAS system (Neuralynx Inc., Montana, USA). We recorded bilaterally from the amygdala, hippocampus,

576 and parahippocampus, and other regions outside the medial temporal lobe. Electrode locations

577 were determined by co-registering postoperative CT and preoperative MRI scans using

578 Freesurfer's mri_robust_register[47]. Each Behnke-Fried electrode shank had 8 microwires on the

579 tip and were marked as one anatomical location. To assess potential anatomical specificity

580 across different participants, we aligned each participant's preoperative MRI scan to the

581 CIT168 template brain in MNI152 coordinates [48] using a concatenation of an affine

582 transformation followed by a symmetric image normalization (SyN) diffeomorphic transform[49].

583 The fifty electrodes within the medial temporal lobe across all the participants are illustrated

584 on the CIT168 template brain in Fig. 1e, with corresponding MNI coordinates listed in

585 Supplementary Table 2.

586

587 **Spike sorting and quality metrics of single units**

588 Spike sorting was performed offline using a semi-automated template matching algorithm

589 Osort[50]. See Zheng et al. 2022 for more details on spike sorting procedures. We identified 1103

590 neurons in this dataset across all brain areasconsidered. As an accurate assesment of phase

591 precession requires a sufficient number of spikes, we excluded 207 neurons with low firing

592 rates (< 0.5Hz) and analyzed the remaining 936 neurons (503 neurons in the medial temporal

593 lobe). The quality of our spike sorting results was evaluated using our standard set of spike

594 sorting quality metrices[51,52] for all considered 936 putative single neurons (Supplementary Fig.

595 1).

596

597 **Characteristics of theta oscillations**

598 Pre-processing: Local field potentials (LFP) were recorded simultaneously with single neuron

599 activity and was used for computing phase precession along with the spike activity from

600 neurons detected from the same microwire. To eliminate potential influences of the spike

601 waveform on the higher frequency parts of the LFP[53], we replaced the LFP in a 3ms long time

602 window centered on the detected spike by linear interpolation. We then downsampled this

603 spike-free version of the LFP from 32kHz to 250Hz, followed by further post-processing using

604   automatic artifact rejection[54] and manual visual inspection using function *fr_databrowser.m*

605   from Fieldtrip toolbox[55]. Trials with large transient signal changes were removed from further

606   analyses. Examples of pre-processed LFP are shown in Fig. 2a, 2c, 2e and gray lines in Fig. 2g

607   and 2i.

608   <u>Spectral analysis</u>: The power spectra (1-20Hz) of the pre-processed LFP were computed using

609   Welch's method (function *pwelch.m* in MATLAB) with Hamming windows (50% overlap). In

610   Fig. 2k and 2n, we performed the spectral analysis on the pre-processed LFP within the 0 to 1

611   seconds time window that follows boundaries in boundary clips.

612   <u>Theta bouts detection</u>: To examine the cycle-to-cycle variability of theta oscillations, we

613   detected transient theta bouts using the method described in previous papers[27,29]. Briefly, first

614   two versions of the LFP were computed: one low-pass filtered at 40Hz ("low-passed LFP") for

615   identifying peaks and troughs in a "smooth" version of LFP without high frequency

616   components; and one band-pass filtered within the theta range (2-10Hz, "theta-filtered LFP")

617   to identify zero-crossings as searching windows for theta bouts detection. Theta bouts (2-10Hz)

618   were identified as time periods in which all detected cycles had similar amplitudes

619   (amp_consistency_threshold = 0.6), similar periods (period_consistency_threshold = 0.6), and

620   relatively symmetric rise and decay flanks (monotonicity_threshold = 0.6) for more than three

621   consecutive putative cycles in time. The frequency of theta bouts was computed as the ratio of

622   how many cycles the theta bout had divided by how long in seconds it lasted. For example, a

623   theta bout that lasted for 2 seconds with 4 cycles had a frequency of 2Hz. The time ratio of theta

624   bouts was computed as how much time of the analysis window was occupied by theta bouts

625   divided by the total length of the analysis window. For example, a theta bout that appeared for

626   1 second out of a 2-second time window had a time ratio of 0.5.

627   <u>Spike phase estimation</u>: Based on the peaks, troughs and zero-crossings identified as described

628   above, we estimated theta phase at all points of time by linearly interpolating between the peaks

629   (0º or 360º), troughs (180º) and zero-crossings (90º or 270º) cycle by cycle. Compared to a

630   conventional Hilbert transform approach, this phase-interpolation method eliminates potential

631   distortions introduced when estimating the phase of non-sinusoidal LFPs[27,56]. To reduce nose

632   in the phase estimation, which is critical for phase precession analysis, we excluded spikes that

633   occurred during the lowest 25th percentile of theta power distribution[16]. The phase assigned to

634   a given spike was set equal to the phase estimated at the point at which the action potential was

635   at its peak.

636

637   **Phase precession measurements**

638   Spike-phase circular linear correlation method (Method 1): We analyzed spikes that occurred

639   within the first three theta cycles following boundaries during encoding or the onset of image

640   display during scene recognition and time discrimination. Phase precession was quantified

641   using circular statistics. For each neuron, we computed the circular-linear correlation

642   coefficient [31] between the spike phase (circular) and time in unwrapped theta phases (linear).

643   Unwrapped theta phase was defined as accumulated cycle-by-cycle theta phase from the

644   alignment point, such as boundary. To assess statistical significance, we generated a null

645   distribution for each circular-linear correlation using surrogate data generated from shuffling

646   neurons spike timing for 1000 times. This procedure maintained the firing rate and spike phase

647   distribution of each neuron while scrambling the correspondence between the spike phase and

648   spike time within each trial. A neuron was considered as a significant phase precession neuron

649   if the observed circular linear correlation exceeded the 95th percentile ($p < 0.05$) of the surrogate

650   null distribution of the correlation coefficient.

651   Chance level of neurons showing phase precession: We estimated the number of neurons

652   exhibiting significant phase precession by chance by recomputing the spike-phase circular-

653   linear correlation 1000 times using the surrogate data generated by shuffling trial numbers

654   between the spike phases and LFP. For each iteration, we obtained the proportion of selected

655   phase precession cells relative to the total number of neurons within each brain region. These

656   1000 values formed the empirically estimated null distribution for the proportion of phase

657   precession cells expected by chance. A brain region was considered to have a significant

658   amount of boundary cells or event cells if its actual fraction of significant cells exceeded 95%

659   of the null distribution (Fig. 5a; $p < 0.05$).

660 **Control analyses for phase precession**

661 We performed following control analyses to further understand the observed phase precession

662 phenomena in our study.

663 <u>Phase precession with different theta cycle numbers</u>: we re-assessed phase precession while

664 varying the number of theta cycles (3 cycles *vs.* 4 cycles) from which the spikes were included

665 for the same analyses. We found that more theta cycles resulted in more spikes included for the

666 analyses but did not significantly affect the proportion of cells exhibiting phase precession (3

667 cycles *vs.* 4 cycles comparison, encoding: $\chi^2 = 5.17$, $p = 0.5$, scene recognition: $\chi^2 = 7.32$, $p =$

668 0.25, time discrimination: $\chi^2 = 6.22$, $p = 0.3$, chi-square test).

669 <u>Phase precession within various analyses windows</u>: we evaluated the prevalence of phase

670 precession by computing the spike-phase circular linear correlation at various task windows

671 (Fig. 3e-g). For example, first three theta cycles after 4-second of no boundary clips, baseline,

672 clip onsets and clip offsets in all the clips, and image offsets during scene recognition and time

673 discrimination.

674 <u>Phase precession using spike-phase autocorrelation method (Method 2)</u>: To examine the

675 robustness of the observed phase precession, we employed a second method to further estimate

676 phase precession based on comparing the autocorrelation of spiking of each neuron with the

677 frequency of the underlying LFP [32]. This alternative method is widely used in rodents[57,58] with

678 stereotypical 8Hz theta, and also in animals with nonstationary theta, such as bats[16], non-human

679 primates[59-61] and humans[17]. For each neuron, we assigned to each spike its unwrapped theta

680 phase by accumulating the cycle-by-cycle phase following boundary during encoding. We

681 computed the autocorrelation ('phase autocorrelation') of these cumulative spiking phases of

682 the spike-train, using 60° bins with window length of 3 cycles. If a neuron exhibits phase

683 precession, its firing phases will occur more and more ahead of theta cycles [32]. In other words,

684 its spike phase autoccorelation will have peaks at a higher rate than the theta cycles

685 (Supplementary Fig. 3f and 3h). To measure this, we fitted decaying sine wave functions to the

686 spike phase autocorrelation for visualization and computed the power spectra of the fitted lines

687 using Fourier transform. The result was presented as a power spectral density plot of the relative

688 frequency ratio between the spiking frequency and the theta frequency. Based on the obtained

689 power spectrum density plot (insets in Supplementary Fig. 3e-3h), we computed the modulation

690 index[17], defined as the amplitude of the power spectra peak normalized by the total amplitude

691 across all other relative frequencies. We then generated a null distribution of modulation indices

692   from spike phase autocorrelations based on surrogate data generated using the same shuffling

693   procedure discussed in spike-phase circular linear correlation. A neuron was considered as

694   exhibiting significant phase precession if its observed modulation index exceeded the 95th

695   percentile of the surrogate distribution. To eliminate potential bias from low spike counts, we

696   only analyzed neurons with more than 80 spikes within the analysis windows across trials for

697   computing spike phase autocorrelation. Further, neurons showing significant phase-locking (p

698   < 0.05, Rayleigh test) and a peak relative frequency around 1 (0.95 to 1.05) were excluded to

699   ensure that we did not mistakenly identify phase locking neurons as exhibiting phase

700   precession. Comparing the neurons selected as phase precessing between Method 1&2 shows

701   significant agreement in which neurons are selected. For example, during encoding, 70% of the

702   neurons selected as phase precessing with Method 1 were also selected with Method 2 (48/68,

703   70.5%; see Supplementary Table 3).

704   <u>Phase precession using absolute time versus time in unwrapped theta phases</u>: we recomputed

705   phase precession using time in second instead of time in unwrapped theta phases for both

706   Method 1 and Method 2 (Supplementary Fig. 3e and 3g). We recomputed the circular-linear

707   correlation and modulation index from spike-time autocorrelation histogram within the 0 to 1-

708   second time window after boundaries during encoding and after the onsets of image display

709   during scene recognition and time discrimination. The alternative measurement using time in

710   seconds resulted in the identification of a smaller number of phase precession cells as compared

711   to our analyses using time in unwrapped theta phase (spike-time correlation vs spike-phase

712   correlation: n = 22 vs 68, χ^2 = 16.6, P < 3x10^{-4}, chi-square test; spike-time autocorrelation vs

713   spike-phase autocorrelation: n = 17 vs 51, χ^2 = 14.7, P < 7 x 10^{-3}, chi-square test). The

714   differences of correlation coefficients when computing using time in unwrapped theta phases

715   versus using time in seconds increased along with the variance of theta bouts' frequency across

716   trials (Supplementary Fig. 3k and 3l). In other words, the approach using time in unwrapped

717   theta phases was sensitive and appropriate for capturing phase precession when LFPs oscillated

718   at a broad theta frequency range across trials.

719

720   **Firing rate modulation**

721   For neurons showing significant phase precession during encoding and retrieval, we computed

722   their average firing rates within the same analysis time windows for computing phase

723   precession - three cycles after boundaries during encoding and after image onsets after scene

724   recognition and time discrimination. A neuron was considered having firing rate modulation if

725   its average firing rate significantly differed between post versus pre analysis time windows (p

726   < 0.05, paired two-tailed t-test). We also assessed the overlap between neurons showing firing

727   rate modulation and phase precession at different task stages (Fig. 5b-d).

728

729   **Relationship between phase precession and memory performance**

730   Generalized linear model: We assessed the relationship between neural metrics (firing rate,

731   phase precession) and participants' memory as assessed behaviorally using a generalized linear

732   model (GLM). Using scene recognition as an example, we grouped trials into the two categories

733   "correctly recognized" and "incorrectly recognized" depending on the accuracy of their

734   response. To account for the difference in trial numbers, we subsampled correct trials with the

735   same trial number as incorrect trials. We first computed phase precession (spike-phase circular-

736   linear correlation) and average firing rates (z-scored normalized to the baseline) within three

737   theta cycles relative to cognitive boundaries during encoding and relative to image onsets

738   during scene recognition, separately for correct and incorrect trials. For each neuron, this

739   resulted in four values each for correct and incorrect trials: correlation coefficients specifying

740   phase precession strength ($r_{encoding}$, $r_{sceneRecog}$) and normalized firing rates ($Fr_{encoding}$, $Fr_{sceneRecog}$).

741   We used a mixed-effect GLM using the function $fitglme.m$ from MATLAB with logistic

742   regression and Bernoulli distribution to predict participants' binary memory outcomes (i.e.,

743   correct vs incorrect) during scene recognition. The fixed effects were different combinations of

744   the four values ($r_{encoding}$, $r_{sceneRecog}$, $Fr_{encoding}$, $Fr_{sceneRecog}$) from all the neurons in the medial

745   temporal lobe. The random effects were neuron ID nested within session ID.

746   Contribution of different fixed effects: To assess the extent to which firing rates and phase

747   precession predicted behavior, we compared different reduced versions of above GLM model.

748   We compared model 1 (fixed effect: $Fr_{encoding}$) with model 2 (fixed effect: model 1 + $Fr_{sceneRecog}$),

749   model 3 (fixed effect: model 1 + $r_{encoding}$), and model 4 (fixed effect: model 1 + $r_{sceneRecog}$). We

750   also added the effect of phase precession during memory retrieval ($r_{sceneRecog}$) to model 3 and

751   compared the model performance between the two. Model comparisons were performed based

752   on the Akaike information criteria, expressed as a log likelihood ratio in Fig. 6a. We did this

753   separately also for the time discrimination task, in which all variables were replaced by the

754   equivalent for the time discrimination task (Fig. 6b). We quantified the strength of each fixed

755   effect using odds ratios to test if they have strong relationship with participants' correct

756   responses during scene recognition and time discrimination. For neurons (n = 77) showing

757   phase precession during encoding or/and scene recognition, we evaluated whether they show

758   significant phase precession or firing rate modulation for trials they correctly versus failed to

759   recognize tested images. An odds ratio is defined as follow.

760

$$odd\ ratio = \frac{\frac{P\ (number\ of\ cells\ with\ effect\ |\ correct)}{P\ (number\ of\ cells\ without\ effect\ |\ correct)}}{\frac{P\ (number\ of\ cells\ with\ effect\ |\ incorrect)}{P\ (number\ of\ cell\ without\ effect\ |\ incorrect)}}$$

761   Effect here refers to one of the following: significant firing rate modulation during encoding

762   ($Fr_{encoding}$) or scene recognition ($Fr_{sceneRecog}$), significant phase precession during encoding

763   ($r_{encoding}$) or scene recognition ($r_{sceneRecog}$). We then performed a Wald test (function waldtest.m

764   from MATLAB) to access the significance of computed odds ratio. As shown in Fig.6c,

765   significant odds ratio bigger than 1 indicated that participants more likely got correct when

766   the given effect was present. We applied same methods for time discrimination as well (Fig.

767   6d).

768   <u>Contribution of different cell groups:</u> We then assessed the ability of different groups of neurons

769   in predicting participants' memory outcomes (correct vs incorrect). To do so we fit the same

770   GLM model 4 as described above (fixed effects: $r_{encoding} + Fr_{encoding} + r_{sceneRecog}$ or $r_{timeDiscrim}$) but

771   including only the neurons who showed phase precession during encoding, only neurons

772   showing phase precession during scene recognition or time discrimination, and the non-phase

773   precession neurons. We then computed the R-squared ratio as the ratio between the R-squared

774   value of GLM Model 4 using different subgroups of neurons $R^2_{sub-groups}$ versus all medial

775   temporal lobe neurons R^2_{All}, as follow:

776

$$R - squared\ ratio = \frac{R^2_{sub-groups}}{R^2_{All}}$$

777   We subsampled the non-phase precession neurons to balance the number of neurons across

778   different subgroups when building the GLM models.

779

780   **Statistical methods and software**

781   Participants were not informed of the existence of cognitive boundaries in the clips. All the

782   statistical analyses were conducted in MATLAB, primarily using the Statistics and Machine

783   Learning toolbox. For comparison against specific values, we used one-sample t-test. For

784   comparison between two groups, we primarily used the Kolmogorov–Smirnov test while for

785   omnibus testing, we used ANOVA, unless otherwise specified in the text. When the normality

786   of dataset was not clear, non-parametric permutation tests were used to determine the

787   significance level by comparing the real test-statistic to the null distribution estimated from

788   surrogate dataset.

789

790

Patient ID	Particip-ant ID	Age	Gender	Number of detected neurons							
				All neurons		Phase precession neurons *Encoding*		Phase precession neurons *SceneRecog*		Phase precession neurons *TimeDiscrim*	
				Inside MTL	Outside MTL	Inside MTL	Outside MTL	Inside MTL	Outside MTL	Inside MTL	Outside MTL
P60CS	1	67	Male	43	27	4	1	3	1	5	1
P61CS	2	52	Female	45	29	5	1	3	0	7	1
TWH101	3	25	Female	31	19	0	0	0	0	0	0
TWH103	4	49	Male	35	22	4	2	2	1	4	1
TWH109	5	28	Male	30	19	3	0	3	1	5	1
TWH110	6	38	Male	19	12	0	0	1	0	0	0
TWH111	7	63	Female	34	21	5	3	4	1	6	2
P62CS	8	25	Female	31	20	2	0	0	0	4	0
TWH113	9	36	Male	33	21	5	2	4	1	6	1
TWH116	10	25	Female	27	17	3	1	3	1	5	1
TWH117	11	68	Female	14	7	2	0	3	0	0	0
P64CS	12	63	Female	28	42	4	3	3	0	6	1
P65CS	13	55	Female	48	30	6	3	4	2	6	1
TWH120	14	25	Female	30	19	5	0	4	1	7	0
TWH125	15	24	Male	31	20	4	1	4	1	5	0
TWH126	16	25	Male	14	8	0	0	0	0	2	0
TWH127	17	28	Male	27	17	2	0	1	0	0	0
TWH129	18	25	Female	29	18	3	2	2	1	5	2
TWH138	19	46	Female	16	10	0	0	0	0	2	0
P70CS	20	30	Female	21	46	4	3	3	1	5	0
P71CS	21	40	Male	24	32	4	0	3	0	5	1
P76CS	22	24	Female	17	20	3	1	1	0	4	0

791 **Supplementary Table 1**. Participants' demographics.

792

793

Electrode ID	PatientID	Location	Side	MNI coordinates		
				X	Y	Z
1	TWH101	Hippocampus	Left	-20.98	-23.8	-13.93
2	P64CS	Hippocampus	Left	-20.44	-17.61	-11.61
3	P60CS	Hippocampus	Left	-27.09	-16.5	-14.95
4	TWH109	Hippocampus	Left	-26.63	-21.1	-16.32
5	TWH110	Hippocampus	Left	-24.98	-17	-15.19
6	TWH111	Hippocampus	Left	-27.58	-22.29	-15.66
7	TWH113	Hippocampus	Left	-20.98	-25.81	-16.33
8	TWH116	Hippocampus	Left	-24.22	-18.17	-18.11
9	TWH125	Hippocampus	Left	-22	-22.81	-20.9
10	TWH129	Hippocampus	Left	-23.11	-18.17	-15.77
11	P70CS	Hippocampus	Left	-20.42	-24.85	-12.02
12	P71CS	Hippocampus	Left	-21.97	-17.84	-5.84
13	P76CS	Hippocampus	Left	-23.35	-19.58	-19.57
14	TWH103	Hippocampus	Right	26.63	-15.83	-16.49
15	TWH109	Hippocampus	Right	24.8	-11.73	-15.77
16	P61CS	Hippocampus	Right	35.99	-19.49	-17.69
17	P62CS	Hippocampus	Right	32.05	-26.82	-6.36
18	TWH116	Hippocampus	Right	24.22	-15.24	-19.28
19	TWH120	Hippocampus	Right	29.38	-14.6	-22.86
20	TWH129	Hippocampus	Right	26.62	-11.81	-20.9
21	TWH138	Hippocampus	Right	31.88	-20.64	-14.63
22	P70CS	Hippocampus	Right	32.21	-21.39	-10.69
23	P71CS	Hippocampus	Right	22.12	-15.1	-13.93
24	P76CS	Hippocampus	Right	23.12	-20.06	-21.7
25	TWH111	Amygdala	Left	-22.63	-2.78	-19.59
26	P64CS	Amygdala	Left	-19.09	-4.89	-17.3
27	P65CS	Amygdala	Left	-18	-3.08	-15.11
28	TWH113	Amygdala	Left	-20.18	-7.39	-14.55
29	TWH125	Amygdala	Left	-23.87	-5.52	-24.23
30	TWH127	Amygdala	Left	-20.07	-6.35	-18.93
31	P70CS	Amygdala	Left	-13.2	-8.71	-18.01
32	P71CS	Amygdala	Left	-13.76	-5.96	-12.93
33	P76CS	Amygdala	Left	-21.55	-4.58	-17.14
34	P60CS	Amygdala	Right	21.89	-2.1	-20.98
35	TWH109	Amygdala	Right	19.93	-3.77	-16.14
36	TWH113	Amygdala	Right	23.32	-4.19	-17.92
37	TWH120	Amygdala	Right	21.78	-4.59	-24.17
38	TWH127	Amygdala	Right	21.46	-3.92	-18.43
39	P70CS	Amygdala	Right	25.82	-9.78	-18.28
40	P71CS	Amygdala	Right	14.52	-2.91	-10.85
41	P76CS	Amygdala	Right	20.99	-4.05	-18
42	P61CS	Parahippocampus	Left	-28.26	-34.91	-8.78
43	TWH117	Parahippocampus	Left	-17.65	-29.59	-15.66
44	TWH120	Parahippocampus	Left	-21.38	-30.21	-18.28
45	TWH125	Parahippocampus	Left	-18.57	-38.31	-16.98
46	TWH127	Parahippocampus	Left	-22	-27.85	-21.33
47	TWH129	Parahippocampus	Left	-17.95	-33.95	-6.57
48	TWH125	Parahippocampus	Right	23.89	-28.71	-21.82
49	TWH126	Parahippocampus	Right	17.41	-28.87	-10.16
50	TWH127	Parahippocampus	Right	17.94	-29.65	-9.66

794 **Supplementary Table 2**. Electrode locations. MNI coordinates of microwire bundles in the medial

795 temporal lobe.

796

797

798

|	Encoding	Scene recognition	Time discrimination
Method 1: Circular linear correlation	68	51	89
Method 2: Spike-phase autocorrelation	51	42	73
Overlap between both methods	48/68 (70.5%)	36/51 (70.6%)	68/89 (76.4%)

799

800 **Supplementary Table 3**. **Method comparison.** Number of phase precession neurons detected during
801 different task stages using the two different methods spike-phase correlation and spike-phase
802 autocorrelation. The bottom row shows the agreement between the two methods (neurons selected by
803 both).

804

805

806
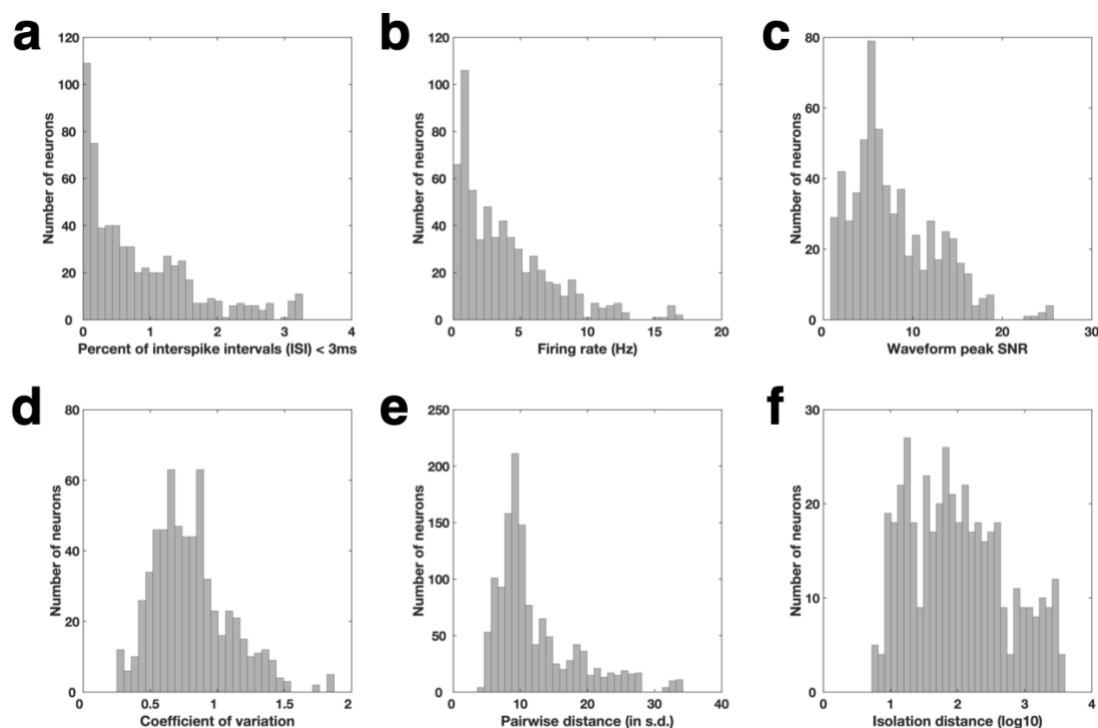
807 **Supplementary Fig. 1 |** Spike sorting quality metrics for all identified putative single cells with firing

808 rates bigger than 0.5 Hz. (a) Proportion of inter-spike intervals (ISI) that were shorter than 3ms. (b)

809 Average firing rate within the entire recording session for all identified putative single cells. (c)

810 Waveform peak signal-to-noise ratio (SNR), which is the ratio between the peak amplitude of the mean

811 waveform and the s.d. of the noise of each identified putative single cell ($8.00 \pm 4,73$, mean $\pm$ s.d.). (d)

812 Coefficient-of-variation (CV2) in the ISI for each identified putative single cell (0.74 ± 0.24, mean $\pm$

813 s.d.). (e) Pairwise isolation distance between putative single cells identified from the same wire. (f)

814 Isolation distance across all identified putative single cells that was calculated in a ten-dimensional

815 feature space of the energy normalized waveforms.

816
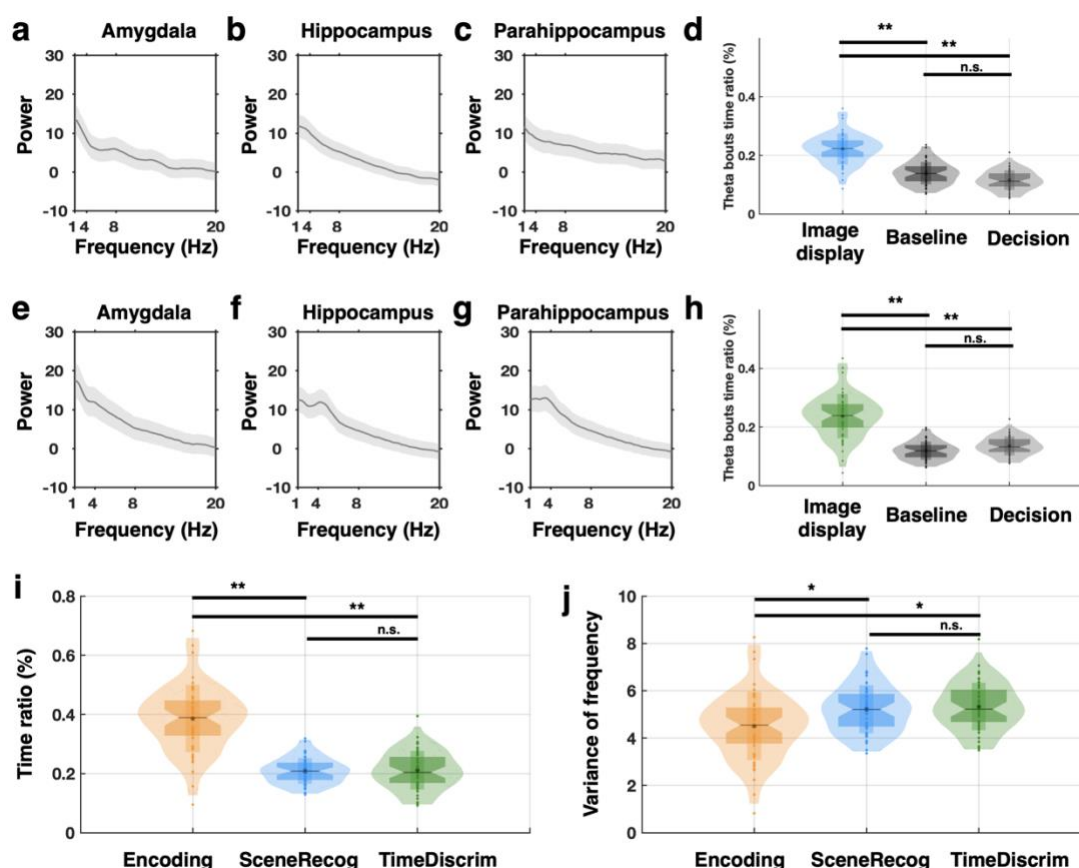
Supplementary Fig. 2 | Comparison of theta bout properties between task stages. **(a-c)** Power spectra of local field potentials recorded during scene recognition averaged across all microelectrodes and the entire task within the indicated brain area. The shaded area indicates the standard error mean. (e-g) Same, but for time discrimination. **(d** and **h)** Proportion of the 1s long analysis window occupied by theta bouts during following the onset of image, baseline, and probe (decision) during scene recognition (d) and time discrimination (h). **(i)** Proportion of time that theta bouts occupy 0 to 1-second after cognitive boundaries (encoding) or after image display (sceneRecog and timeDiscrim). (**j**) Comparison of the variance of frequency for theta bouts that are detected within the 0 to 1-second after cognitive boundaries (encoding) or after image display (sceneRecog and timeDiscrim). * $p < 0.05$, ** $p < 0.01$, *** $p < 0.001$, n.s. = not significant.

829
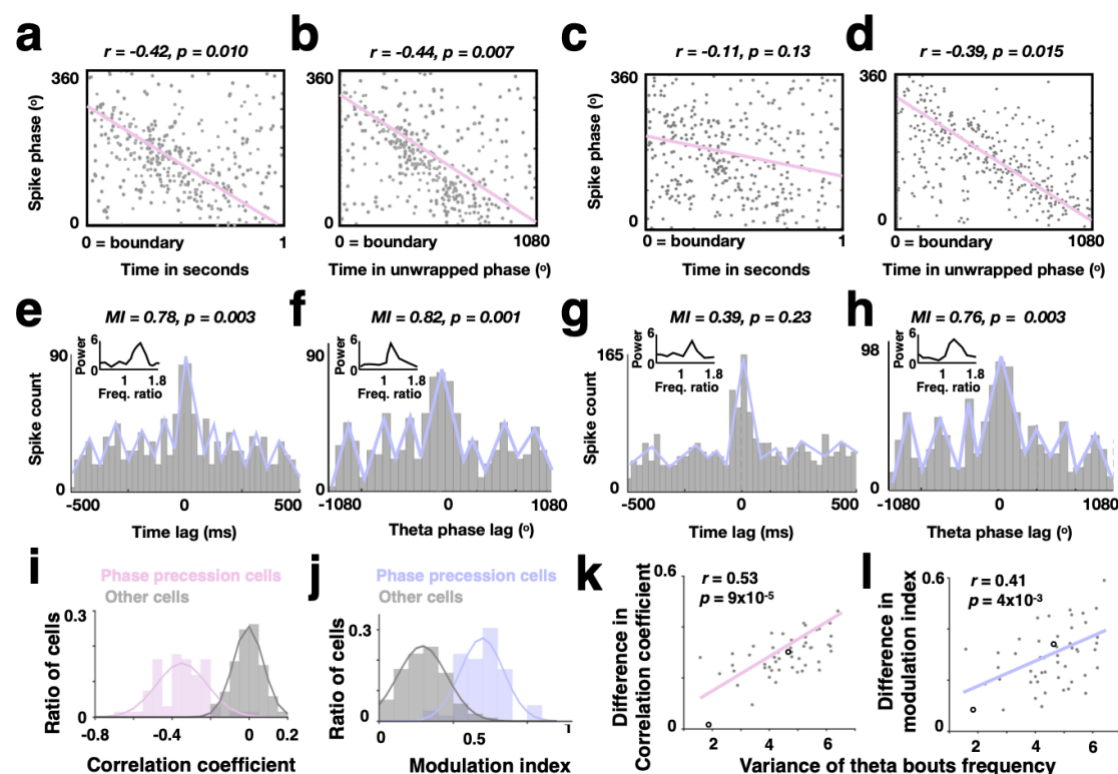
830 **Supplementary Fig. 3 |** Phase precession quantified using the method 1 and 2. **(a-d)** Two example
831 hippocampal neurons' (recorded on the microelectrodes shown in Fig. 2g and 2i). Spike phases (relative
832 to theta oscillations) are plotted as a function of time in seconds (a and c; method 1) or time in unwrapped
833 theta phases (b and d; method 2), aligned to cognitive boundaries. Phase precession is quantified as the
834 circular-linear correlations between neuronal spiking phases and time in seconds (a and c; method 1) or
835 time in unwrapped theta phases (b and d; method 2). Pink lines indicate the correlation, with the
836 correlation value and its statistical significance listed on the top of each subplot. **(e-h)** Further
837 calculations for Method 2. The spike-time autocorrelation (e and g) and spike-phase autocorrelation (f
838 and h) plots for the same neurons in (a-d). Blue lines indicate the decaying sine wave function fitted to
839 the autocorrelation plots. Inset shows the spike-phase spectra, with power as the y-axis and the relative
840 frequency between the frequency of spiking and frequency of heta oscillations as the x-axis. Phase
841 precession is quantified using the modulation index (MI), which is defined as the fraction between the
842 peak height divided by the area under the curve in the spike-phase spectra plot. The modulation index
843 and its statistical significance are listed on the top of each subplot. (**i** and **j**) Correlation coefficients (i)
844 and modulation indices (j) for significant (pink) versus non-significant (gray) phase precession neurons.
845 (**k**) Differences in correlation coefficient (e.g., $|r$ in b $- r$ in a$|$) against the frequency variance of theta
846 bouts detected in these microelectrodes for significant neurons during encoding. (**l**) Differences in
847 modulation index (l, e.g., $|MI$ in f $- MI$ in e$|$) against the frequency variance of theta bouts detected in
848 these microelectrodes for significant neurons during encoding. In k and l, each dot represents one neuron.
849 The empty circle represents the two example neurons in (a-h). Color lines indicate the fitted linear
850 regression, with the correlation value and its statistical significance listed on the top of each plot.

851

852
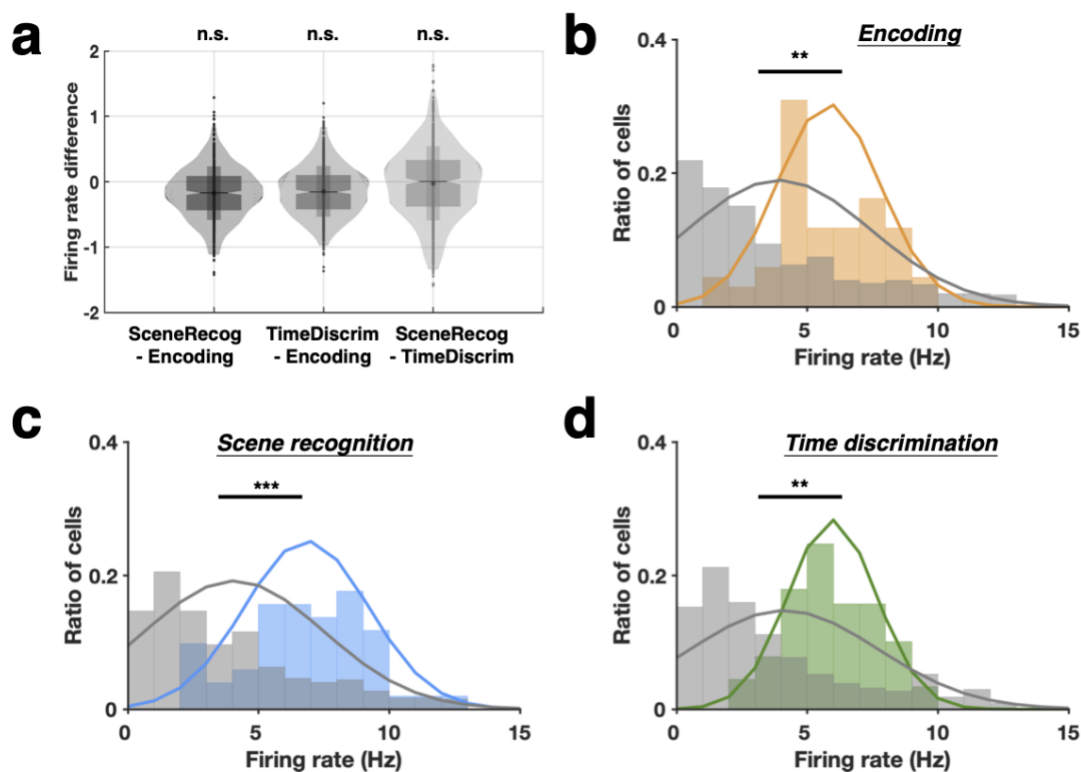
853 **Supplementary Fig. 4 |** Firing rates of phase precession neurons. **(a)** For phase precession neurons (n =
854 117), their firing rates averaged within the 0 to 1-second time window after cognitive boundaries
855 (encoding) and image display (scene recognition and time discrimination) are compared across different
856 task stages. **(b-d)** Firing rates of neurons with (color) and without phase precession (gray) averaged
857 within 0 to 1-second time window after cognitive boundaries during encoding (b), image display during
858 scene recognition (c), and image display during time discrimination (d).

859

860
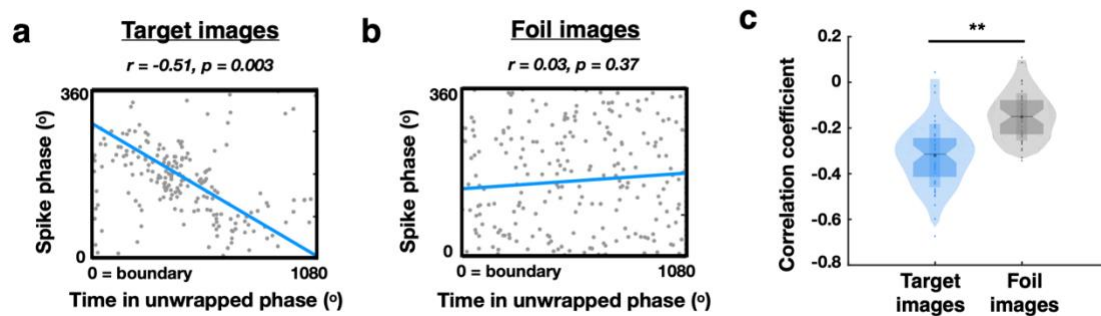
861 **Supplementary Fig. 5 |** Comparison of phase precession when recognizing target versus foil images. **(a**

862 and **b)** An example MTL neuron showing phase precession when the participant is asked to recall

863 recognize target images (a) while no phase precession is observed when identifying foil images (b). (c)

864 Comparison between phase precession strength (correlation coefficient values) when participants are

865 instructed to recognize target (blue) versus foil images (gray) across all phase precession neurons

866 identified during scene recognition (n = 51). Each dot represents one neuron. The shaded violin shape

867 represents the data distribution with lower end of 1st percentile and top end of 99th percentile. The top

868 edge and bottom edge of the shaded rectangle represent the mean ± std., respectively. **$p< 0.01$, n.s. =

869 not significant.

870

Reference

1   Lisman, J. E. & Jensen, O. The theta-gamma neural code. *Neuron* **77**, 1002-1016, doi:10.1016/j.neuron.2013.03.007 (2013).

2   Lisman, J. E. & Idiart, M. A. Storage of 7 +/- 2 short-term memories in oscillatory subcycles. *Science* **267**, 1512-1515, doi:10.1126/science.7878473 (1995).

3   Hopfield, J. J. Pattern recognition computation using action potential timing for stimulus representation. *Nature* **376**, 33-36, doi:10.1038/376033a0 (1995).

4   Bi, G. & Poo, M. Synaptic modification by correlated activity: Hebb's postulate revisited. *Annu Rev Neurosci* **24**, 139-166, doi:10.1146/annurev.neuro.24.1.139 (2001).

5   Jensen, O. & Lisman, J. E. Position reconstruction from an ensemble of hippocampal place cells: contribution of theta phase coding. *J Neurophysiol* **83**, 2602-2609, doi:10.1152/jn.2000.83.5.2602 (2000).

6   Terada, S., Sakurai, Y., Nakahara, H. & Fujisawa, S. Temporal and Rate Coding for Discrete Event Sequences in the Hippocampus. *Neuron* **94**, 1248-1262 e1244, doi:10.1016/j.neuron.2017.05.024 (2017).

7   Kaminski, J., Brzezicka, A., Mamelak, A. N. & Rutishauser, U. Combined Phase-Rate Coding by Persistently Active Neurons as a Mechanism for Maintaining Multiple Items in Working Memory in Humans. *Neuron* **106**, 256-264 e253, doi:10.1016/j.neuron.2020.01.032 (2020).

8   Buzsaki, G. & Tingley, D. Space and Time: The Hippocampus as a Sequence Generator. *Trends Cogn Sci* **22**, 853-869, doi:10.1016/j.tics.2018.07.006 (2018).

9   Liebe, S. *et al.* Phase of firing does not reflect temporal order in sequence memory of humans and recurrent neural networks. *bioRxiv*, 2022.2009.2025.509370, doi:10.1101/2022.09.25.509370 (2022).

10   Takahashi, M., Nishida, H., Redish, A. D. & Lauwereyns, J. Theta phase shift in spike timing and modulation of gamma oscillation: a dynamic code for spatial alternation during fixation in rat hippocampal area CA1. *J Neurophysiol* **111**, 1601-1614, doi:10.1152/jn.00395.2013 (2014).

11   O'Keefe, J. & Recce, M. L. Phase relationship between hippocampal place units and the EEG theta rhythm. *Hippocampus* **3**, 317-330, doi:10.1002/hipo.450030307 (1993).

12   Dragoi, G. & Buzsaki, G. Temporal encoding of place sequences by hippocampal cell assemblies. *Neuron* **50**, 145-157, doi:10.1016/j.neuron.2006.02.023 (2006).

13   Skaggs, W. E., McNaughton, B. L., Wilson, M. A. & Barnes, C. A. Theta phase precession in hippocampal neuronal populations and the compression of temporal sequences. *Hippocampus* **6**, 149-172, doi:10.1002/(SICI)1098-1063(1996)6:2<149::AID-HIPO6>3.0.CO;2-K (1996).

14   Danjo, T., Toyoizumi, T. & Fujisawa, S. Spatial representations of self and other in the hippocampus. *Science* **359**, 213-218, doi:10.1126/science.aao3898 (2018).

15   Courellis, H. S. *et al.* Spatial encoding in primate hippocampus during free navigation. *PLoS Biol* **17**, e3000546, doi:10.1371/journal.pbio.3000546 (2019).

16   Eliav, T. *et al.* Nonoscillatory Phase Coding and Synchronization in the Bat Hippocampal Formation. *Cell* **175**, 1119-1130 e1115, doi:10.1016/j.cell.2018.09.017 (2018).

17   Qasim, S. E., Fried, I. & Jacobs, J. Phase precession in the human hippocampus and entorhinal cortex. *Cell* **184**, 3242-3255 e3210, doi:10.1016/j.cell.2021.04.017 (2021).

18   Reddy, L. *et al.* Theta-phase dependent neuronal coding during sequence learning in human single neurons. *Nat Commun* **12**, 4839, doi:10.1038/s41467-021-25150-0 (2021).

19   Aronov, D., Nevers, R. & Tank, D. W. Mapping of a non-spatial dimension by the hippocampal-entorhinal circuit. *Nature* **543**, 719-722, doi:10.1038/nature21692 (2017).

20   Harris, K. D. *et al.* Spike train dynamics predicts theta-related phase precession in hippocampal pyramidal cells. *Nature* **417**, 738-741, doi:10.1038/nature00808 (2002).

21   Pastalkova, E., Itskov, V., Amarasingham, A. & Buzsaki, G. Internally generated cell assembly sequences in the rat hippocampus. *Science* **321**, 1322-1327, doi:10.1126/science.1159775 (2008).

22   Lenck-Santini, P. P., Fenton, A. A. & Muller, R. U. Discharge properties of hippocampal neurons during performance of a jump avoidance task. *J Neurosci* **28**, 6773-6786, doi:10.1523/JNEUROSCI.5329-07.2008 (2008).

23   Hasselmo, M. E. & Eichenbaum, H. Hippocampal mechanisms for the context-dependent retrieval of episodes. *Neural Netw* **18**, 1172-1190, doi:10.1016/j.neunet.2005.08.007 (2005).

24   Reifenstein, E. T., Bin Khalid, I. & Kempter, R. Synaptic learning rules for sequence learning. *Elife* **10**, doi:10.7554/eLife.67171 (2021).

25   Umbach, G. *et al.* Time cells in the human hippocampus and entorhinal cortex support episodic memory. *Proc Natl Acad Sci U S A* **117**, 28463-28474, doi:10.1073/pnas.2013250117 (2020).

26   Zheng, J. *et al.* Neurons detect cognitive boundaries to structure episodic memories in humans. *Nat Neurosci* **25**, 358-368, doi:10.1038/s41593-022-01020-w (2022).

27   Cole, S. & Voytek, B. Cycle-by-cycle analysis of neural oscillations. *J Neurophysiol* **122**, 849-861, doi:10.1152/jn.00273.2019 (2019).

28   Aghajan Z.M. *et al.* Theta Oscillations in the Human Medial Temporal Lobe during Real-World Ambulatory Movement. *Curr Biol* **27**, 3743-3751 e3743, doi:10.1016/j.cub.2017.10.062 (2017).

29   Penner, C., Minxha, J., Chandravadia, N., Mamelak, A. N. & Rutishauser, U. Properties and hemispheric differences of theta oscillations in the human hippocampus. *Hippocampus* **32**, 335-341, doi:10.1002/hipo.23412 (2022).

30   Reifenstein, E. T., Kempter, R., Schreiber, S., Stemmler, M. B. & Herz, A. V. Grid cells in rat entorhinal cortex encode physical space with independent firing fields and phase precession at the single-trial level. *Proc Natl Acad Sci U S A* **109**, 6301-6306, doi:10.1073/pnas.1109599109 (2012).

31   Kempter, R., Leibold, C., Buzsaki, G., Diba, K. & Schmidt, R. Quantifying circular-linear associations: hippocampal phase precession. *J Neurosci Methods* **207**, 113-124, doi:10.1016/j.jneumeth.2012.03.007 (2012).

32   Mizuseki, K., Sirota, A., Pastalkova, E. & Buzsaki, G. Theta oscillations provide temporal windows for local circuit computation in the entorhinal-hippocampal loop. *Neuron* **64**, 267-280, doi:10.1016/j.neuron.2009.08.037 (2009).

33   Petersen, P. C. & Buzsaki, G. Cooling of Medial Septum Reveals Theta Phase Lag Coordination of Hippocampal Cell Assemblies. *Neuron* **107**, 731-744 e733, doi:10.1016/j.neuron.2020.05.023 (2020).

34   Royer, S., Sirota, A., Patel, J. & Buzsaki, G. Distinct representations and theta dynamics in dorsal and ventral hippocampus. *J Neurosci* **30**, 1777-1787, doi:10.1523/JNEUROSCI.4681-09.2010 (2010).

35   van der Meer, M. A. & Redish, A. D. Theta phase precession in rat ventral striatum links place and reward information. *J Neurosci* **31**, 2843-2854, doi:10.1523/JNEUROSCI.4869-10.2011 (2011).

36   Schlesiger, M. I. *et al.* The medial entorhinal cortex is necessary for temporal organization of hippocampal neuronal activity. *Nat Neurosci* **18**, 1123-1132, doi:10.1038/nn.4056 (2015).

37   Mehta, M. R., Lee, A. K. & Wilson, M. A. Role of experience and oscillations in transforming a rate code into a temporal code. *Nature* **417**, 741-746, doi:10.1038/nature00807 (2002).

38   Bush, D. & Burgess, N. Advantages and detection of phase coding in the absence of rhythmicity. *Hippocampus* **30**, 745-762, doi:10.1002/hipo.23199 (2020).

39   Jones, M. W. & Wilson, M. A. Theta rhythms coordinate hippocampal-prefrontal interactions in a spatial memory task. *PLoS Biol* **3**, e402, doi:10.1371/journal.pbio.0030402 (2005).

40   Rutishauser, U., Mamelak, A. N. & Schuman, E. M. Single-trial learning of novel stimuli by individual neurons of the human hippocampus-amygdala complex. *Neuron* **49**, 805-813, doi:10.1016/j.neuron.2006.02.015 (2006).

41   Kaminski, J. *et al.* Novelty-Sensitive Dopaminergic Neurons in the Human Substantia Nigra Predict Success of Declarative Memory Formation. *Curr Biol* **28**, 1333-1343 e1334, doi:10.1016/j.cub.2018.03.024 (2018).

42   Wilson, M. A. & McNaughton, B. L. Dynamics of the hippocampal ensemble code for space. *Science* **261**, 1055-1058, doi:10.1126/science.8351520 (1993).

43   Huxter, J., Burgess, N. & O'Keefe, J. Independent rate and temporal coding in hippocampal pyramidal cells. *Nature* **425**, 828-832, doi:10.1038/nature02058 (2003).

44   Foster, D. J. & Wilson, M. A. Hippocampal theta sequences. *Hippocampus* **17**, 1093-1099, doi:10.1002/hipo.20345 (2007).

45   O'Keefe, J. & Burgess, N. Dual phase and rate coding in hippocampal place cells: theoretical significance and relationship to entorhinal grid cells. *Hippocampus* **15**, 853-866, doi:10.1002/hipo.20115 (2005).

46   Robinson, N. T. M. *et al.* Medial Entorhinal Cortex Selectively Supports Temporal Coding by Hippocampal Neurons. *Neuron* **94**, 677-688 e676, doi:10.1016/j.neuron.2017.04.003 (2017).

47   Reuter, M., Rosas, H. D. & Fischl, B. Highly accurate inverse consistent registration: a robust approach. *Neuroimage* **53**, 1181-1196, doi:10.1016/j.neuroimage.2010.07.020 (2010).

48   Pauli, W. M., Nili, A. N. & Tyszka, J. M. A high-resolution probabilistic in vivo atlas of human subcortical brain nuclei. *Sci Data* **5**, 180063, doi:10.1038/sdata.2018.63 (2018).

49   Avants, B. B., Epstein, C. L., Grossman, M. & Gee, J. C. Symmetric diffeomorphic image registration with cross-correlation: evaluating automated labeling of elderly and neurodegenerative brain. *Med Image Anal* **12**, 26-41, doi:10.1016/j.media.2007.06.004 (2008).

50   Rutishauser, U., Schuman, E. M. & Mamelak, A. N. Online detection and sorting of extracellularly recorded action potentials in human medial temporal lobe recordings, in vivo. *J Neurosci Methods* **154**, 204-224, doi:10.1016/j.jneumeth.2005.12.033 (2006).

51   Kaminski, J. *et al.* Persistently active neurons in human medial frontal and medial temporal lobe support working memory. *Nat Neurosci* **20**, 590-601, doi:10.1038/nn.4509 (2017).

52   Pouzat, C., Mazor, O. & Laurent, G. Using noise signature to optimize spike-sorting and to assess neuronal classification quality. *J Neurosci Methods* **122**, 43-57, doi:10.1016/s0165-0270(02)00276-5 (2002).

53   Anastassiou, C. A., Perin, R., Buzsaki, G., Markram, H. & Koch, C. Cell type- and activity-dependent extracellular correlates of intracellular spiking. *J Neurophysiol* **114**, 608-623, doi:10.1152/jn.00628.2014 (2015).

54   Banaie Boroujeni, K., Tiesinga, P. & Womelsdorf, T. Adaptive spike-artifact removal from local field potentials uncovers prominent beta and gamma band neuronal synchronization. *J Neurosci Methods* **330**, 108485, doi:10.1016/j.jneumeth.2019.108485 (2020).

55   Oostenveld, R., Fries, P., Maris, E. & Schoffelen, J. M. FieldTrip: Open source software for advanced analysis of MEG, EEG, and invasive electrophysiological data. *Comput Intell Neurosci* **2011**, 156869, doi:10.1155/2011/156869 (2011).

56   Belluscio, M. A., Mizuseki, K., Schmidt, R., Kempter, R. & Buzsaki, G. Cross-frequency phase-phase coupling between theta and gamma oscillations in the hippocampus. *J Neurosci* **32**, 423-435, doi:10.1523/JNEUROSCI.4122-11.2012 (2012).

57   Geisler, C. *et al.* Temporal delays among place cells determine the frequency of population theta oscillations in the hippocampus. *Proc Natl Acad Sci U S A* **107**, 7957-7962, doi:10.1073/pnas.0912478107 (2010).

58   Kim, S. M., Ganguli, S. & Frank, L. M. Spatial information outflow from the hippocampal circuit: distributed spatial coding and phase precession in the subiculum. *J Neurosci* **32**, 11539-11558, doi:10.1523/JNEUROSCI.5942-11.2012 (2012).

59   Stewart, M. & Fox, S. E. Hippocampal theta activity in monkeys. *Brain Res* **538**, 59-63, doi:10.1016/0006-8993(91)90376-7 (1991).

60   Killian, N. J., Jutras, M. J. & Buffalo, E. A. A map of visual space in the primate entorhinal cortex. *Nature* **491**, 761-764, doi:10.1038/nature11587 (2012).

61   Jutras, M. J., Fries, P. & Buffalo, E. A. Oscillatory activity in the monkey hippocampus during visual exploration and memory formation. *Proc Natl Acad Sci U S A* **110**, 13144-13149, doi:10.1073/pnas.1302351110 (2013).